Department of Precision and Microsystems Engineering

A plucking based frequency up-converted vibration energy harvesting method

Rutger Ham

Report no : 2021.031
Coach : Thijs Blad
Professor : Farbod Alijani
Specialisation : Engineering Dynamics
Type of report : MSc thesis report
Date : 1 June 2021

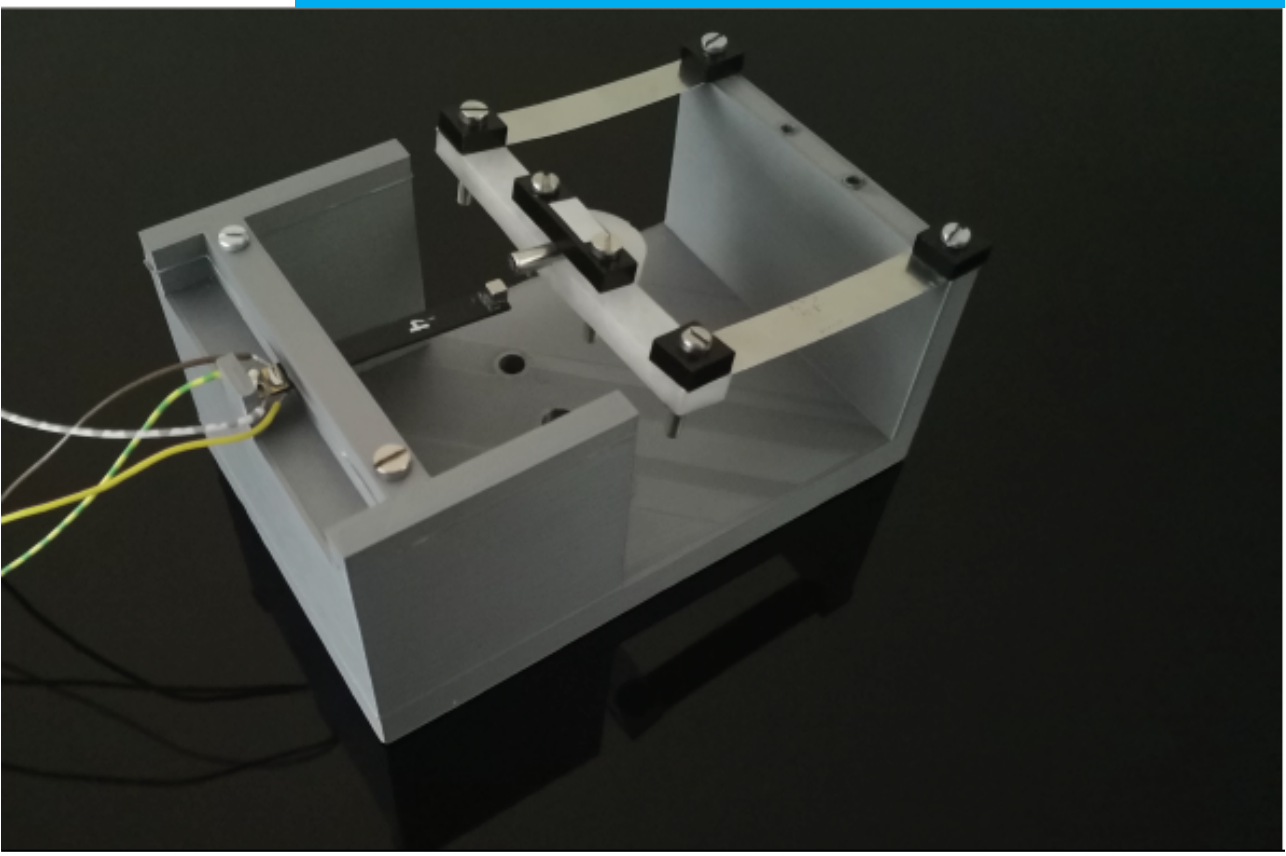

TU Delft Delft University of Technology

Challenge the future

A PLUCKING BASED FREQUENCY UP-CONVERTED VIBRATION ENERGY HARVESTING METHOD

A PLUCKING BASED FREQUENCY UP-CONVERTED VIBRATION ENERGY HARVESTING METHOD

MSc Thesis

In partial fulfillment of the requirements for the degree of Master of Science in Mechanical Engineering. To be defended on 1 June 2021.

by

Rutger HAM

Report number: 2021.031
Daily supervisor: Ir. T.W.A. Blad
Senior supervisor: Dr. F. Alijani

This thesis was approved by the following committee:

Dr. F. Alijani,	Technische Universiteit Delft
Dr. D. Farhadi Machekposhti,	Technische Universiteit Delft
Ir. T. W. A. Blad,	Technische Universiteit Delft

Keywords: Vibration energy harvesting, frequency up-conversion, piezoelectricity, modal analysis, experimental validation
Front: Rutger Ham

An electronic version of this thesis report is available at
http://repository.tudelft.nl/.

I'm going on a journey, and bring along.
You.

G. De Randamie

SUMMARY

Vibration energy harvesting has proven to be a durable source of energy for a wide variety of applications, however not all of the positions these applications are placed at are suitable for conventional vibration energy harvesting. For some of these applications a frequency up-converted energy harvester could increase the power harvested. These systems are analysed in this thesis project, by first gaining insight in previously performed work in chapter 2. In order to contribute to the development of this type of energy harvesters a new design is introduced in chapter 3. The new design consists of two cantilever beams connected to a shared base with a magnetic non-contact coupling between them. One of these beams is mainly oscillating at the input motion frequency, while the second cantilever beam is oscillating at its natural frequency and is a piezoelectric beam in order to transduce energy. The model for this system is described using a distributed parameter model based on modal analysis to describe the governing equations. Together with a model to have a proper description of the magnetic coupling forces in order to describe the complete system. This model is found in chapter 3. After which the results of the experiments are described in chapter 4. Lastly the thesis project is discussed in chapter 5, which consist of an overview of the research activities, a discussion of the results found during the project, along with recommendations for future works, and finally the conclusions drawn during the thesis project.

CONTENTS

1

INTRODUCTION

This first chapter will provide an introduction to frequency up-converted energy harvesting and the reason why it is a field worthy exploring. It will show the challenges that are faced with vibration energy harvesting methods. The chapter will also introduce the problem statement which has been addressed during the research project.

The modern society requires electrical energy which has been obtained from different sources throughout the years. Fossil fuels are widely used, but the current energy transition requires more sustainable sources of energy. Often these are thought of as wind, water, or soler energy, however ambient energy sources have also been identified. Heat is a widely used ambient energy source, however a more recently explored energy source has been found in vibrations and motion. This vibration energy comes from the motion induced by the system from which it can be harvested, think of machines with a vibration, cars going over bumps, or the up and down motion which happens while you walk. These energy sources can be used to power systems nearby, but should not be interfering with the source of the motion significantly. Examples of devices to be powered could be wrist watches or monitoring sensors attached to humans or machines.These use cases have been mostly powered by batteries in the past. For certain applications the battery maintenance has proven to be costly, which further provides reasoning to incorporate a method of vibration energy harvesting.

Applications where vibration energy harvesting may become the main source of energy can be described as sensor applications in hard or expensive to connect places like a tyre on a car, the sides of a train railways, or devices placed on humans. These can be used to monitor the current state of the environment of these systems, in order to predict failure or warn for dangerous circumstances. These devices can also provide continuous measurement instead of periodic checks, which will further enhance the decision for the proper actions to be taken in due time. These apply for both industrial applications, as well as medical applications such as pacemakers or patient monitoring sensors. Both the previously mentioned costs, as well as the challenges that arise from replacing the battery or an entire device after these have been depleted sustain the choice of charg-

1

ing while in use. This is where vibration energy harvesting has been shown to form a solution for these applications.

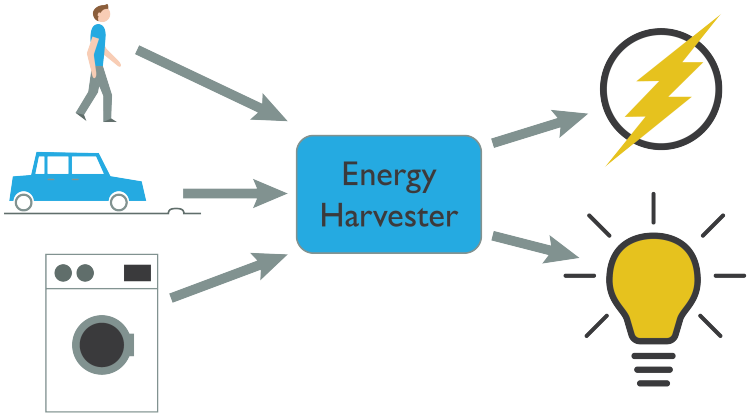

Figure 1.1: The principle goal of vibration energy harvesting. Vibrations from ambient sources working on an energy harvester will be transduced into electrical power.

1.1. VIBRATION ENERGY HARVESTING

Now as to how this vibration energy harvesting works may differ from system to system, however some common traits are observed. The source of the energy are the mechanical vibrations, to which the devices are subjected merely by their attachment position. A basic vibration energy harvester is described as an oscillator whose damping causes electromechanical transduction to convert motion into electrical energy. A schematic of such a system can be found in figure 1.2.

In this system the body is moved by a base motion. The oscillation is a reaction of the spring with stiffness to the inertia of mass, which will naturally damp out due to mechanical damping. However, another damping factor is introduced for energy harvesting which transduces the motion energy into electrical energy. For this transducer three different types are commonly identified in vibration energy harvesters, namely piezoelectric, electromagnetic, and electrostatic.

These systems can be implemented in certain systems as it is, however when certain constraints are introduced different solutions may be found in order to optimise the performance of these energy harvesters. One such constraint is the dimension in the direction of oscillation, which has a significant impact on the performance of the energy harvester as discussed by Blad [1]. Another variable to take into consideration is the input motion, which can be a large variety of signals. Examples of these are sinusoidal motion, impact based signals, or random noise vibrations. In this thesis the focus will be on harmonic motion, which can often be used to described the governing motion in the previously discussed applications.

These common constraints raise a challenge for which a solution needs to be found. This thesis explores one such solution, where together with one oscillator moving at the

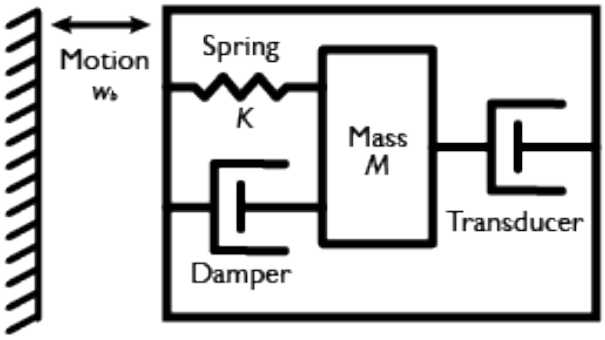

Figure 1.2: Schematic overview of a single oscillating vibration energy harvester.

same frequency as the base motion another oscillator is introduced. This second oscillator is set in motion at a higher frequency where the transduction into electrical energy is performed. This in turn results in a lower required amplitude of motion of the system. These systems have been named frequency up-converted energy harvesters.

1.2. FREQUENCY UP-CONVERTERS

Frequency up-converted energy harvesters (FupC) consist of two oscillators, one which is predominantly set in motion by the base motion at a frequency similar to this motion while the second oscillator is set in motion by an interaction with the first oscillator at its natural frequency. Three basic layouts of these frequency up-converted energy harvesters can be identified, which are schematically presented in figure 1.3. Where the low frequency oscillator (LFO) is the oscillator which oscillates at a frequency similar to the input motion, while the high frequency oscillator (HFO) is set in motion by the up-conversion interaction.

These FupC methods are found in literature, for which a small sample of solutions is seen in figure 1.4. These are later further analysed in chapter 2. However, these do give an overview of different solutions that have been found on top of which this research is housed.

1.3. RESEARCH OBJECTIVE

During this thesis project first a set of FupC specific design parameters were identified during the literature review. The focus of the majority of the thesis project was to identify the effects of the frequency up-converted specific design variables, however it was found this goal would not contribute to the development of FupC systems in general. Instead the focus shifted towards presenting the newly designed frequency up-converted energy harvesting method.

A new frequency up-converted energy harvester design is presented, which fits in the gap current frequency up-converted energy harvesters have left open. For this FupC

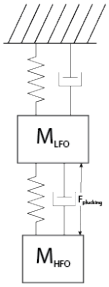

(a) HFO on top of the LFO with an up-conversion interaction between both oscillators.

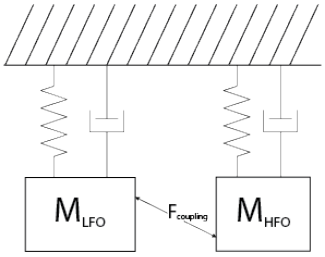

(b) HFO connected to the base, while the up-conversion happens between the oscillators.

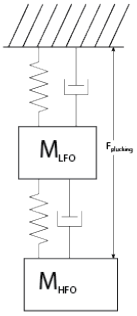

(c) HFO connected to the LFO with an up-conversion happening due to interaction with the base.

Figure 1.3: Three configuration for frequency up-converters. Differing by the up-conversion interaction and the position of the high frequency oscillator (HFO).

design a model is also introduced which can be used in future designs and work. This new design is fabricated and experimentally validated to show it is able to perform the frequency up-conversion. However, first a comparison of presented FupC prototypes based on the identified FupC specific design parameters is shown.

REFERENCES

[1] T. W. Blad and N. Tolou, *On the efficiency of energy harvesters: A classification of dynamics in miniaturized generators under low-frequency excitation,* Journal of Intelligent Material Systems and Structures **30**, 2436 (2019).

[2] T. Galchev, E. E. Aktakka, and K. Najafi, *A Piezoelectric Parametric Frequency Increased Generator for Harvesting Low-Frequency Vibrations,* Journal of Microelectromechanical Systems **21**, 1311 (2012).

[3] S. Ju and C.-H. Ji, *Impact-based piezoelectric vibration energy harvester,* Applied Energy **214**, 139 (2018).

[4] B. Andò, S. Baglio, V. Marletta, A. Pistorio, and A. R. Bulsara, *A low-threshold bistable device for energy scavenging from wideband mechanical vibrations,* IEEE Transactions on Instrumentation and Measurement **68**, 280 (2019).

[5] E. Dechant, F. Fedulov, D. V. Chashin, L. Y. Fetisov, Y. K. Fetisov, and M. Shamonin, *Low-frequency, broadband vibration energy harvester using coupled oscillators and*

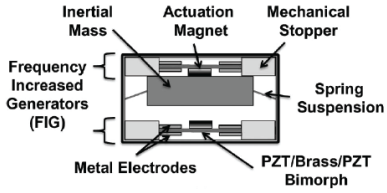

(a) Galchev et al. [2]

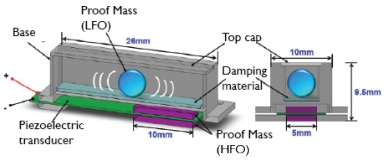

(b) Ju et al. [3]

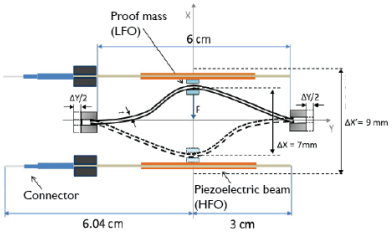

(c) Ando et al. [4]

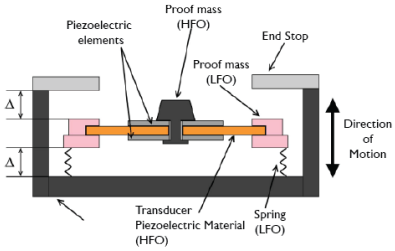

(d) Dechant et al. [5]

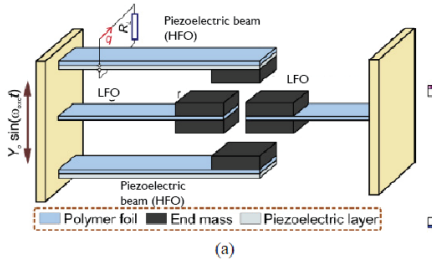

(e) Dauksevicius et al. [6]

Figure 1.4: A sample set of FupC designs presented in literature. The red dots show the positions of the low frequency oscillators, while the blue dots show the positions of the high frequency oscillators. The individual captions consist of the source of the shown FupC.

frequency up-conversion by mechanical stoppers, Smart Materials and Structures **26**, 065021 (2017).

[6] R. Dauksevicius, D. Briand, R. Lockhart, A. V. Quintero, N. de Rooij, R. Gaidys, and V. Ostasevicius, *Frequency up-converting Vibration Energy Harvester with Multiple Impacting Beams for Enhanced Wideband Operation at Low Frequencies,* Procedia Engineering **87**, 1517 (2014).

2

Literature Review: Frequency up conversion principles for energy harvesting: A Classification

In the field of motion energy harvesting a specific domain is found that has its main focus on capturing low frequency motion. This low frequency motion energy can not be efficiently harvested without increasing the frequency. This is done using frequency up converters. These converters have been designed and analysed in the past, however a framework to identify has been missing. In this paper these existing systems will be identified and they will be categorised. After this their performance will be classified based on introduced metrics. Newly identified specific design variables found for frequency up-converted energy harvesters are shown, and their relation to the performance metrics will be shown. The introduced frequency ratio is found to have a strong relation to the bandwidth.

2.1. Introduction

Current medical devices and sensors are powered by batteries that have to be replaced periodically.[1] These replacement costs are expensive as this replacement often requires surgery. Extending the lifetime of these devices would thus be beneficial to both the cost aspect as well as the user comfort. One way of extending the lifetime of these devices is to recharge the batteries as the devices are in use. A field that is currently being explored in order to do this is motion energy harvesting, where the movement of the body is also used to power these electronic devices.

The field of motion energy harvesting is broad, as a wide variety of applications has been found. The design criteria of these energy harvesters depend on the limitations on their dimensions, but also on the input motion to these devices. High frequency

systems found in industrial factories produce motion that can be efficiently harvested using systems identified by Vullers et al. [2]. These systems often use resonating motion in the system to efficiently harvest energy, this may cause a problem for devices that are designed to harvest energy from human motion. These systems often can not use resonance, as the input motion is much larger than the size of the harvester.

One solution to this problem is found in frequency up-converted energy harvesters. These systems use two oscillators, where a low frequency oscillator is moving at the same frequency as the input motion while a high frequency oscillator is activated by the previously mentioned low frequency oscillator. This up conversion causes a higher frequency, at which a lower amplitude of the motion is required to get a similar energy capacity. Previously several frequency up-converted energy harvesters (FupC) have been presented. These FupC have been designed for frequencies below 100Hz, with a motion that is larger than the system.

However, the presented systems are hard to compare amongst one another. Different FupCs have been presented but their designs vary widely, while the tests conducted are also different. A method of comparing systems in order to identify stengths and weaknesses of specific design choices is therefore required.

The goal of this classification is thus to present the research that has been conducted in the field of FupCs and to identify FupC specific design variables which can be related to the performance of the systems.

First the comparison criteria for FupCs is presented, these include performance parameters and newly introduced FupC specific design variables. After which the method of obtaining a set of presented systems is presented. These result in a found classification, which is then presented. The results for the found systems are then shown, after which these are discussed. This discussion is followed up by the recommendations. After which this is summarised in the conclusion.

2.2. METHOD

In order to make a comparison of FupC a set of presented systems had to be found, the progress and criteria for the presented systems will be described first. This set of presented systems should be compared against one another, this should be done using the data that is available. The parameters and metrics that are used for comparison will be introduced second, together with FupC specific design variables.

2.2.1. PERFORMANCE EVALUATION

In order to compare the experimental results of different devices there are various performance metrics that can be used. For energy harvesters in general a number of metrics have already been presented by Blad [3], Mitchesson [4], and Liu [5]. The presented metrics for performance represent the efficiency and the bandwidth. A choice for both of these performance metrics has to be made and will be discussed, first the efficiency after which the bandwidth will be discussed.

EFFICIENCY

A number of metrics were presented to discuss the efficiency of different energy harvesters. These efficiency metrics can also be applied to FupCs. The volume figure of

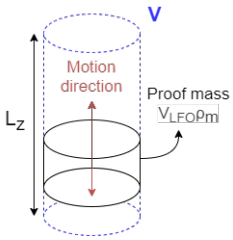

Figure 2.1: Imaginary energy harvesters proof mass with the input motion direction showing. The total volume in which the proof mass can move is denoted by V, while the volume of the proof mass itself is denoted by V_{LFO}. Multiplied with the proof mass density, denoted by ρ_M, this will result in the mass of the proof mass. The dimension in the direction of the driving motion is denoted by L_z.

merit (FoM_V) presented by [4] results in a method to compare energy harvesters of different sizes and types under harmonic excitation. The metric describes the ratio between the useful power output of the harvester and the maximum power output of an imaginary harvester cube of the same volume, driven by the same vibration conditions. As a baseline the proof mass of this imaginary harvester is assumed to have the density of gold. As the bandwidth will be discussed separately, a combined figure of merit is not desired which has been proposed by Liu [5].

As the FoM_V does take the total volume of the generator into account it does not take any dimensions of this volume into account. However, these dimensions are important as the dimension parallel to the driving motion has a higher impact on the power output. This is the reasoning behind the improved FoM_G presented by Blad [3]. Also, the proof mass density is not assumed to be gold but to be the density of the used proof mass. This will also benefit systems for which a high density material was not readily available, as well as to decrease the benefit systems that have a high density material as proof mass.

The generator figure of merit fully depends on the design of the energy harvester. The generator figure of merit is the ratio of the average output power divided by the maximum output power that can be produced by the energy harvester. The full expression for the generator figure of merit is as follows

$$FoM_G = \frac{P_{avg}}{\frac{1}{16} Y_0 \rho_M V L_Z \omega^3} \tag{2.1}$$

Where P_{avg} is the average output power measured in experiments, Y_0 and ω are the amplitude and frequency of the driving motion respectively. The value ρ_M is the density of the proof mass material, while V is the total volume the system occupies. The L_Z value is the maximum length the proof mass can travel, which is visualised in figure 2.1. In the case of a frequency up converter there are two proof masses, the proof mass that has been measured for the previously named values is the proof mass of the low frequency up converter.

The value used in this comparison is the peak efficiency.

NORMALISED HALF EFFICIENCY BANDWIDTH

Most presented experimental work present the power output over a frequency range, which is typically obtained using a frequency sweep with constant acceleration. This

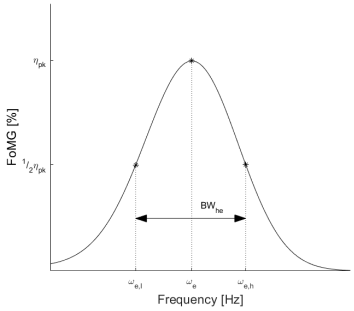

Figure 2.2: Example graph for the FoM_G against frequency. The peak efficiency (η_{pk}) and the corresponding frequency (ω_e) are shown as well as the half efficiency bandwidth (BW_{he}) and its limits ($\omega_{e,l}$ and $\omega_{e,r}$).

data can then be used to determine the efficiency over this frequency range. The newly found data can then be used to determine a bandwidth. The bandwidth measure that will be used for this classification is the normalised half-efficiency bandwidth. Where the frequency width at half of the peak efficiency is used, which is then normalised by the frequency at which the efficiency peak is found. This is visualised in figure 2.2, where the BW_{he} is the half efficiency bandwidth and the frequency at the peak efficiency is ω_e. The resulting bandwidth equation can thus be summarised as equation 2.2

$$BW_{nhe} = \frac{BW_{he}}{\omega_e} = \frac{\omega_{e,h} - \omega_{e,l}}{\omega_e} \tag{2.2}$$

2.2.2. INPUT MOTION EVALUATION

For an overview of the current field of FupCs the input motion was also reviewed, as this should give an insight in the range for which these FupCs are currently designed. This input motion was found to be harmonic for all experimental work, and thus can be described based on the acceleration and frequency of the input motion. The acceleration and frequency are also used to determine the amplitude of the driving motion Y_0, using equation 2.3. Where a is the acceleration and f is the frequency.

$$Y_0 = \frac{a}{f^2} \tag{2.3}$$

2.2.3. ENERGY HARVESTER DESIGN VARIABLE

As previously mentioned the L_Z value has a large contribution to the efficiency of these systems. This L_Z value is often limited, while systems for which it is not limited can make use of resonance. Thus for energy harvesters the motion ratio was introduced to determine whether they can make use of resonance.

MOTION RATIO

As it is assumed that FupCs are mostly going to be used in cases where the size of the harvester is small compared to the driving motion applied to the system another inter-

esting metric is the motion ratio. In these cases resonance induced amplification of the motion can not be used. Therefore looking into the ratio between the motion range of the proof mass compared to the motion range of the driving motion is interesting to decide whether a frequency up-converted system should be efficient. The motion ratio is defined by Blad [3] as follows

$$\lambda = \frac{L_Z}{2Y_0} \tag{2.4}$$

Where L_Z and Y_0 are the motion ranges of the low frequency oscillator proof mass and the driving motion, respectively. In order to be able to make use of resonance the statement $L_Z >> Y_0$ must be true, thus low motion ratios are to be expected for FupCs.

2.2.4. FREQUENCY UP-CONVERTED SPECIFIC DESIGN VARIABLES

Previously a design variable for the energy harvesters was identified. However, such design variables that are specific to FupCs were not yet identified. The following FupC specific design variables are introduced.

MASS RATIO

In FupCs there are two proof masses, namely those of the low frequency oscillator and the high frequency oscillator. In order to determine whether the choice of the masses has an effect a mass ratio is chosen. In order to normalize the values the ratio between a proof mass of the high frequency oscillator and the combined weight of the low frequency oscillator and high frequency oscillators is taken. If there are multiple high frequency oscillators these are all used in the combined weight.

$$\Psi = \frac{M_{HFO}}{M_{LFO} + nM_{HFO}} \tag{2.5}$$

Where M_{HFO} and M_{LFO} are the proof masses of the high and low frequency oscillators respectively. The parameter n is the amount of high frequency oscillators.

FREQUENCY RATIO

In order to classify frequency up-converters a frequency ratio is something that should be noted. However, as frequency up-converters do not necessarily use resonance peaks another frequency for the low frequency should be used. This low frequency to use for the frequency ratio is the frequency at which the efficiency peak is found, previously named $\omega_{e,pk}$. For the high frequency oscillator the natural frequency is often given or can be determined from time-displacement graphs. The frequency ratio is then described as follows, which should always result in a value above 1 to be an up converter.

$$\phi = \frac{\omega_{HFO}}{\omega_e} \tag{2.6}$$

2.2.5. LITERATURE SEARCH METHOD

A literature search has been performed on FupCs. Scientific papers were found using Scopus and Google Scholar in the field of FupCs, low frequency energy harvesting, large

motion amplitude energy harvesting, non-resonating energy harvesting, and frequency increased generators. This resulted in a set of presented systems.

Presented systems for which not all performance values and design variables could be found were removed from the mentioned set. This data could often be determined as it was directly reported, estimated from a graph or figure, or had to be calculated. Some systems were tested under different conditions, and can thus be found multiple times in the results. The data that has often been missing was data required to determine the FoM_G, which is also required to determine the bandwidth. The data set on which this classification reports is thus not including all FupCs.

2.3. CLASSIFICATION

FupCs that have been reported vary in design, however they have some traits in common. The frequency up-converters all require two oscillators, which are not kinematically dependent on eachother. Between these two oscillators the frequency up-conversion takes place. The frequency up-conversion principle can be classified based on the following criterion.

2.3.1. HIGH FREQUENCY OSCILLATOR EXCITATION METHOD

As previously described by Blad [3] and Elvin and Erturk [6] a distinguishment can be made between impact and plucking. Where systems using impact excitation have a non-zero velocity, and the transfer involves a transfer of momentum. This can be compared to the striking of the hammers on the wires of a piano. While on the other hand systems that can be identified with plucking excitation have a non-zero displacement, and the transfer of energy is done by a slow, relative to the high frequency, deformation. Which can be compared to the plucking of chords on a guitar.

Typical trajectories of the high oscillator is shown in figures 2.3 and 2.4 for both the impact systems and plucking systems, respectively. It can be seen that a long period is used to displace the high frequency oscillator, relative to the period of the high frequency oscillator. Whereas the impact system is almost instantly deformed.

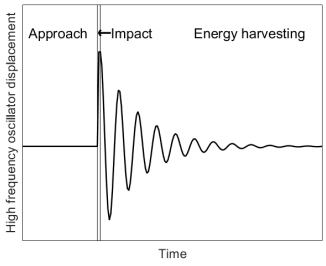

Figure 2.3: Typical motion trajectory of the high frequency oscillator in an impact system. Where the three stages are identified as the approach, impact, and energy harvesting stage.

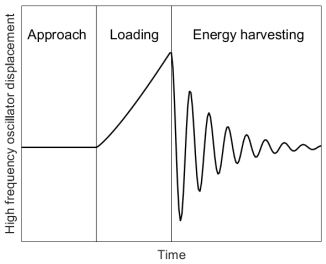

Figure 2.4: Typical motion trajectory of the high frequency oscillator in a plucking system. Where the three stages are identified as the approach, loading, and energy harvesting stage.

Table 2.1: The performance metrics and design variables of the FupCs categorised in the classes impact and plucking.

Class	Motion Ratio (λ)	Peak Efficiency (η_{pk})	Bandwidth (BW_{nhe})	Mass Ratio (Ψ_M)	Frequency Ratio (ϕ_ω)	References
Impact	0.23 - 11.75	0.037 - 0.0676 %	0.070-0.662	0.068 - 0.207	1.93-35.7	Ashraf et al.[7];Dauksevicius et al.[8];Dechant et al.[9];Gu and Livermore[10]
Plucking	0.013 - 22.3	0.0015 - 1.6 %	0.336 - 3.08	0.00065 - 0.041	4.26 - 42.09	Galchev et al.[11];Galchev et al.[12];Pillatsch et al.[13];Tang et al.[14]

2.4. RESULTS

First the input conditions of the tested prototypes are presented. After which the efficiency and bandwidth are presented against the motion ratio. Finally the newly presented FupC specific design variables are used to show their relationship with the efficiency and bandwidth.

2.4.1. INPUT RESULTS

The input motion used for the experimental testing of the systems should give a first insight into the application range of FupCs. The frequencies where the highest efficiency is measured range from 0.16Hz up to 34.9Hz, while the acceleration ranges from 2.7m/s^2 up to 29.43m/s^2. The data points in figure 2.5 show the frequency and acceleration for which the highest efficiency is measured, where the shaded area shows the range of the input motion for both impact and plucking.

2.4.2. PERFORMANCE RESULTS

FupCs have been experimentally tested, these results will be shown hereafter. First these results will be presented against the general energy harvester specific parameter, namely the motion ratio. After which the newly presented FupC specific design variables will be used to present the performance metrics against.

ENERGY HARVESTER SPECIFIC PARAMETER

The motion ratio as introduced by Blad [3] was used to make a first comparison for the performance of both classes. These results can be seen in figures 2.6 and 2.7 for the peak generator figure of merit and the normalised half-efficiency bandwidth respectively. The range of the motion ratio is found to be between 0.013 and 22.3 for the plucking systems, whereas the impact systems range between 0.23 and 11.75. Plucking systems have a peak

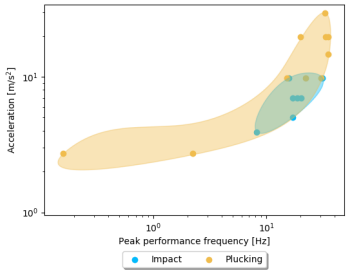

Figure 2.5: Graph showing the data points where the highest efficiency is measured for different input motion expressed in acceleration and frequency of harmonic motion. The categories impact and plucking are shown in different colours, while the shaded area describes the range of values for which experiments were reported.

efficiency between 0.0015% and 1.6%, while impact systems range between 0.037% and 0.0676%. The normalised half-efficiency bandwidth for plucking systems was found to be between 0.336 and 3.08, while impact systems were found between 0.07 and 0.662.

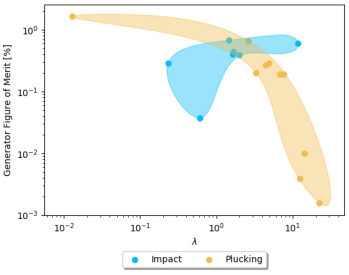

Figure 2.6: Peak efficiency in terms of generator figure of merit (η_{pk}) versus motion ratio (λ) of found FupC systems by up-conversion principle. The shaded areas show the range where systems are reported. The numbers indicate the source referenced in this paper, which can occur multiple times for various conditions.

FUPC SPECIFIC DESIGN VARIABLES

The performance metrics are plotted against the FupC specific design variables. These graphs for the performance metrics against the mass ratio are shown in figures 2.8 and 2.9 for the generator figure of merit and normalised half-efficiency bandwidth respectively. The mass ratio for the plucking systems range between 0.00065 and 0.041, whereas the range for the impact systems is found between 0.0608 and 0.207.

The graphs for the peformance metrics against the frequency ratio are shown in figure 2.11 and 2.10 for the generator figure of merit and the normalised half-efficiency bandwidth. The frequency ratio ranges between 1.93 and 35.7 for the impact systems, while the plucking systems have been found to reach frequency ratios between 4.26 and 42.09.

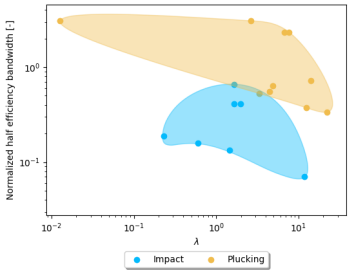

Figure 2.7: Normalised half-efficiency bandwidth (BW_{nhe}) versus motion ratio (λ) of found FupC systems by up-conversion principle. The shaded areas show the range where systems are reported. The numbers indicate the source referenced in this paper, which can occur multiple times for various conditions.

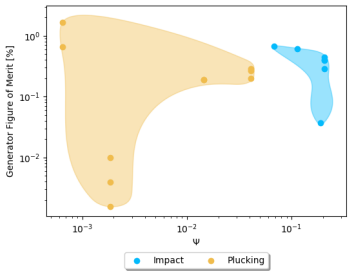

Figure 2.8: Peak efficiency in terms of generator figure of merit (η_{pk}) versus Mass ratio (Ψ) of found FupC systems by up-conversion principle. The shaded areas show the range where systems are reported. The numbers indicate the source referenced in this paper, which can occur multiple times for various conditions.

2.5. DISCUSSION

Current FupC systems are tested for a large range of input motion varying in acceleration and frequency. This is partially caused by the test method, which is often a shaker with a limited motion range. Systems with low acceleration and frequency have to be tested by another method. The input motion for the plucking systems are in a large range, however this is mainly caused by only two systems that are tested at low frequencies. These last two are indeed tested with another method than the conventional shaker.

It can be noted that the highest peak efficiencies for both impact and plucking based systems are comparable. Plucking based systems that have a lower motion ratio are found to return a higher efficiency, however this relation is caused by only few systems. When more systems are tested and evaluated a stronger connection may be found. The widespread range in the performance metrics can be explained by the varying degree of optimisation and quality of the systems, especially their transduction elements and the power conditioning circuitry.

Impact systems are, based on their normalised half-efficiency bandwidth, more limited in their frequency range compared to plucking systems. However, when looking

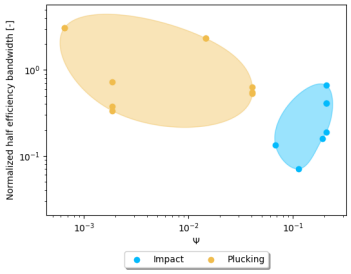

Figure 2.9: Normalised half-efficiency bandwidth (BW_{nhe}) versus Mass ratio (Ψ) of found FupC systems by up-conversion principle. The shaded areas show the range where systems are reported. The numbers indicate the source referenced in this paper, which can occur multiple times for various conditions.

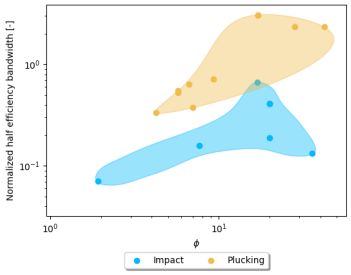

Figure 2.10: Normalised half-efficiency bandwidth (BW_{nhe}) versus Frequency ratio (ϕ) of found FupC systems by up-conversion principle. The shaded areas show the range where systems are reported. The numbers indicate the source referenced in this paper, which can occur multiple times for various conditions.

more in depth it can be seen that some wideband plucking systems have a sudden drop-off to almost no power output outside the bandwidth, while impact systems still work at a low efficiency for a wide range. When this happens for plucking systems it is often seen that snap-through behaviour is not occurring anymore. The same can occur for impact systems that make use of a multi stable system, when the jump between stable positions can not be made anymore.

The mass ratio of impact based systems has been found to be higher than the mass ratio of plucking based systems. Plucking based systems with a high mass ratio make use of magnets on the high frequency oscillator, while some plucking systems do not use any added proof mass on piezoelectric cantilever beams. The high mass ratio of the impact systems has been identified, however from models that have been presented it can be found that high mass ratios are not necessarily more efficient.

When looking at the frequency ratio a relation to the efficiency can not be identified, the contrary can be said about the relation to the bandwidth. For both impact an plucking systems it can be seen that a higher frequency ratio also results in a higher bandwidth. This relation may be interesting to explore more in depth, as systems with

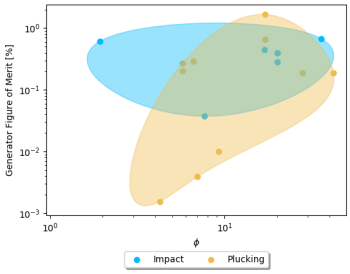

Figure 2.11: Peak efficiency in terms of generator figure of merit (η_{pk}) versus Frequency ratio (ϕ) of found FupC systems by up-conversion principle. The shaded areas show the range where systems are reported. The numbers indicate the source referenced in this paper, which can occur multiple times for various conditions.

higher frequency ratios can be designed. An upper limit to this relation is expected as the vibration of the high frequency oscillator is damped out, however a longer time between the activation of this high frequency oscillator results in a lower required damping which may in turn be the reason for the increase in bandwidth.

2.6. RECOMMENDATIONS

The published data on different prototypes varies widely. In order to properly identify the use cases from future prototypes all required data has to be presented. This data can be put in three different parts.

First information about the prototype has to be presented, this would be fully dependent on the design and fabrication. Data that has to be presented are at least the proof masses, the total mass, the volume of the system, the generator volume which has been previously described, the length of the generator motion, as well as the density of the proof mass. Other data required to reproduce the prototype should obviously also be presented.

The second part for which information has to be supplied is test data. For this a proper test has to be developed, which includes sweeping over a frequency range and preferably also over an acceleration range. This input motion should include the complete bandwidth of the system at every acceleration. The test results should include the average power output from the system. Other outputs that can be presented are the positions over time, especially the HFO with respect to the LFO. The tests should also make clear whether a frequency sweep causes hardening behaviour, this can enable a high power output which in real world applications may never be reached.

The final part which has to be presented for every prototype is the calculated data. These combine both previous parts to determine data which can be used to compare the performance of different systems. These calculated values should at least include the bandwidth and the frequency at which peaks are found. Also an efficiency indicator should be presented, preferably the generator figure of merit.

Different categories can be identified based on the working principles of the frequency up-conversion method. Current research is missing a lot of data on less straight-

forward up-conversion principles. The categories should be independent of one another, where one of the categories is the previously mentioned up conversion principle. Other categories are for example the location of the HFO compared to the LFO, or the connection method between the oscillators. Also for the durability reasons another interesting category may be whether contact, causing wear, is made between the LFO and the HFO.

Future research should benefit from an analysis of the frequency up-converted design variables for similar systems. This can then be used to validate the sensitivity of the performance parameters. Currently impact based systems have a high mass ratio, however systems with a low mass ratio could be interesting to determine the sensitivity of the bandwidth even if a decrease in efficiency is already expected. As such the introduction of new methods and the experimental work on new prototypes is useful for further analysis.

2.7. CONCLUSION

Although FupCs are an active research topic, the unavailability of data for the presented systems limits this classification. The values that are often not presented are the maximum motion length of the low oscillator proof mass (L_Z) and the density of the proof mass. Also, often single frequency test results are shown instead of frequency sweep results.

Future work can focus on systems and conditions with smaller motion ratios, this would also be where FupCs are expected to work better compared to other energy harvesters.

A higher bandwidth is observed for plucking based systems compared to impact based systems. A higher efficiency however is not observed for either class.

The introduced frequency up-converter specific design variables are identified and are shown to have a relation to the performance. As a higher frequency ratio is expected to result in a higher bandwidth.

REFERENCES

[1] E. Romero, *Powering Biomedical Devices* (Elsevier, 2013).

[2] R. J. M. Vullers, R. van Schaijk, I. Doms, C. Van Hoof, and R. Mertens, *Micropower energy harvesting*, Solid-State Electronics Papers Selected from the 38th European Solid-State Device Research Conference – ESSDERC'08, **53**, 684 (2009).

[3] T. Blad and N. Tolou, *On the efficiency of energy harvesters: A classification of dynamics in miniaturized generators under low-frequency excitation*, Journal of Intelligent Material Systems and Structures **30**, 2436–2446 (2019).

[4] P. Mitcheson, E. Yeatman, G. Rao, A. Holmes, and T. Green, *Energy harvesting from human and machine motion for wireless electronic devices*, Proceedings of the IEEE **96**, 1457–1486 (2008).

[5] W. Q. Liu, A. Badel, F. Formosa, and Y. P. Wu, *A new figure of merit for wideband vibration energy harvesters*, Smart Materials and Structures **24**, 125012 (2015).

[6] N. Elvin and A. Erturk, eds., *Advances in energy harvesting methods* (Springer, New York, 2013) oCLC: ocn812252500.

[7] K. Ashraf, M. Md Khir, J. Dennis, and Z. Baharudin, *Improved energy harvesting from low frequency vibrations by resonance amplification at multiple frequencies,* Sensors and Actuators A: Physical **195**, 123 (2013).

[8] R. Dauksevicius, D. Briand, R. Lockhart, A. V. Quintero, N. de Rooij, R. Gaidys, and V. Ostasevicius, *Frequency up-converting Vibration Energy Harvester with Multiple Impacting Beams for Enhanced Wideband Operation at Low Frequencies,* Procedia Engineering **87**, 1517 (2014).

[9] E. Dechant, F. Fedulov, D. V. Chashin, L. Y. Fetisov, Y. K. Fetisov, and M. Shamonin, *Low-frequency, broadband vibration energy harvester using coupled oscillators and frequency up-conversion by mechanical stoppers,* Smart Materials and Structures **26**, 065021 (2017).

[10] L. Gu and C. Livermore, *Impact-driven, frequency up-converting coupled vibration energy harvesting device for low frequency operation,* Smart Materials and Structures **20**, 045004 (2011).

[11] T. Galchev, H. Kim, and K. Najafi, *Micro Power Generator for Harvesting Low-Frequency and Nonperiodic Vibrations,* Journal of Microelectromechanical Systems , 5961600 (2011).

[12] T. Galchev, E. E. Aktakka, and K. Najafi, *A Piezoelectric Parametric Frequency Increased Generator for Harvesting Low-Frequency Vibrations,* Journal of Microelectromechanical Systems **21**, 1311 (2012).

[13] P. Pillatsch, E. M. Yeatman, and A. S. Holmes, *A scalable piezoelectric impulse-excited generator for random low frequency excitation,* in *2012 IEEE 25th International Conference on Micro Electro Mechanical Systems (MEMS)* (IEEE, Paris, France, 2012) pp. 1205–1208.

[14] Q. C. Tang, Y. L. Yang, and X. Li, *Bi-stable frequency up-conversion piezoelectric energy harvester driven by non-contact magnetic repulsion,* Smart Materials and Structures **20**, 125011 (2011).

3

DESIGN AND MODELLING

This chapter will describe the theoretical part of the thesis project. First the design method will be presented, and the design decisions which were made are discussed. After which the design which is developed during this thesis project is presented. This is followed by showing a model for this design based on modal analysis and coupling forces found in literature. This model is then implemented in MATLAB, for which a number of steps were taken in order to problem solve. Finally the results from the implemented MATLAB model are shown and discussed.

During the graduation work a design for a frequency up-converted energy harvester was made. This design had to behave as a frequency up-converter and its goal was to validate a model designed to observe the sensitivity of FupC specific ratios described by the literature review with regards to the performance parameters. This goal was not met, however the resulting design is presented in this work. As such the design process of the prototype is of importance and will be described in this chapter together with the developed model.

The design had to fulfill a number of demands, which will be addressed first. After these goals a set of input parameters will be given for which the FupC will be tested. These parameters and demands were then used to determine the design of the prototype by first looking into the oscillator options and followed by analysing the coupling options. A resulting design will then be addressed including basic calculations to determine design parameters for the prototype. Lastly the prototype bulding method will be described.

The three basic configurations of a FupC are shown in figure 1.3. These three configurations all consist of two oscillators, with a coupling between them in order to perform the frequency up-conversion. The low frequency oscillator (LFO) will be described as the oscillator with the low frequency, which is actuated directly by the input motion. While the high frequency oscillator (HFO) will be coupled to the LFO, which will set the HFO in motion to its natural frequency. This HFO also houses the electromechanical transduction in order to harvest energy from the input motion.

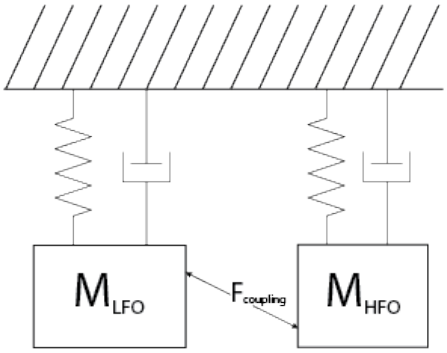

Figure 3.1: Schematic representation of a basic FupC design where the frequency up-conversion happens between the LFO and HFO, and the HFO is connected to the base.

3.1. DEMANDS

As the goal had been to validate a model using this prototype a first demand was the ease of fabrication for this prototype. The prototype should be made using materials and tools available, as well as not take large amounts of time to build while still resulting in proper results that could be used for the validation of the model. This would also increase the adjustability of the design, which is considered a benifit in order to validate the model for different design parameters.

Another demand was found in the FupC behaviour, as having multiple nonlinearities in the prototype may result in a less general model for frequency up-converters. This would result in demanding an oscillator which can be described with linear oscillations, and a nonlinear coupling between the LFO and HFO.

A final demand was described by the experimental setup, which also resulted in design parameters. The experiments will be performed on an electrodynamic shaker, and as such the input motion was required to be above 5Hz as well as a maximum motion amplitude of 30mm. Later it was found the input motion frequency had to be higher in order to have a feedback controlled acceleration amplitude using the available system.

A basic frequency up-converter has been described in chapter 2. The three FupC setups were weighed against one another and the model chosen to work further on during this research has been the model where the frequency up-conversion coupling and the base were the only coupling between the LFO and HFO, which can be seen in figure 3.1. This was chosen as the other designs would have a higher risk of inducing undesired nonlinearities in the coupling and oscillation.

3.2. PARAMETERS

As previously mentioned the experiments will be performed on a motion shaker. As such the weight was limited, as well as the coupling force as a high coupling force would result in high feedback accelerations. The low frequency oscillator will be designed to have a base frequency of 10Hz, while the high frequency oscillator should have a frequency at least 5 times the base frequency. This was chosen in order to perform the experiments as well as to have a significant up-conversion.

Other parameters was the constraint on the motion range of the oscillators. As a large motion ratio, defined in chapter 2, is undesirable for frequency up-converted energy harvesters as other designs may work better for such situations. This would result in a demand where the motion ratio was at most 2.

3.3. OSCILLATOR DESIGN

In order to determine the oscillation method different oscillators were found. These different options are summarised in figure 3.2. Other considerations in the field of compliant mechanisms were dropped early on as these would cause nonlinearities, however should be considered for further research.

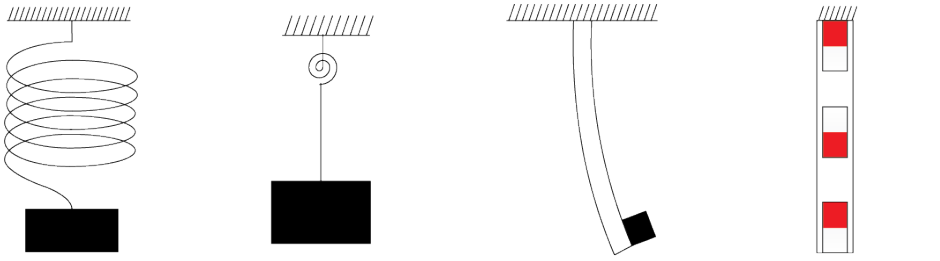

(a) Translational spring (b) Rotational spring (c) Cantilever beam (d) Magnetic balanced oscillator

Figure 3.2: Different oscillator designs considered during the design process.

The magnetic design seen in figure 3.2d is not preferred as the magnetic oscillation is already nonlinear, which is contradicting the previously stated demands. The spring designs are mostly linear over a large range of motion, however while adjusting a spring may seem easy the process of manufacturing is not. As these springs are not readily available in any preferred size this would be an obstacle. Due to ease of adjusting a design for the cantilever beam, as well as having an easier method of connecting the LFO to the HFO this was preferred.

3.4. COUPLING

A number of coupling methods have been found in literature. Where a basic distinction can be made between the impact and plucking behaviours. This clear distinction is extensively described in the previous chapter, as such it will not be further elaborated

on. However, for the design it was determined a plucking based system is preferred as a higher bandwidth was often found, while not penalising the peak efficiency.

Other distinctions have also been identified during this process, such as whether the coupling is contact based. A side effect which is observed in contact based frequency up-converters as seen in the works by Galchev [1] is both a plucking and impact phase often happen, causing nonlinear dynamic behaviour. Also the work by Andò [2] describes another problem with contact based piezoelectric harvesting, namely these impacts often result in increased stresses and may cause cracks when using piezoelectric transducers.

Lastly a distinction has been described by the location of the plucking behaviour compared to the phase of the low frequency oscillator, meaning the up-conversion can happen at either the far ends of the motion the LFO makes or in between. Devices with frequency up-conversion at the limits of the LFO motion are often seen with either buckling systems, as in the works by Andò [2], or magnetic coupling as described by Galchev [3]. These will also behave as end stops for the LFO, and as such will cause non-linearities which are undesired. As such the frequency up-conversion should happen in the high velocity range of the motion made by the LFO.

Different combinations of distinctions can be seen in figure 3.3 in order to give a broad overview of what has been found in literature. From this analysis it was determined a combination of design choices was not yet fulfilled and presented. This was the combination of in-motion non-contact plucking based devices using cantilever beams as oscillators.

(a) Contact based plucking during motion

(b) Non-contact plucking at end

(c) Contact based plucking at end

(d) Non-contact based plucking during motion

Figure 3.3: A subset of different methods of plucking based coupling for frequency up-conversion.

3.5. INITIAL DESIGN

The combination of these factors resulted in an initial design schematic which is seen in figure 3.4. The system consists of two opposing cantilevers, one with a low natural frequency and one with a higher natural frequency. The high frequency oscillator is chosen to be a piezoelectric cantilever beam in order to transduce motion into electrical energy. The coupling is performed by two magnets at the tips of both cantilever beams, these also form a tip mass for the cantilevers.

After this piezoelectric beams were found readily available, on which the design is based. Other factors that were taken into account were the previously mentioned parameters, and as such a low frequency oscillator with a natural uncoupled frequency of 10Hz was designed. A benefit of the design was the interchangeable LFO tip masses in order to adjust the gap size between the magnets. The parameters of the prototype are

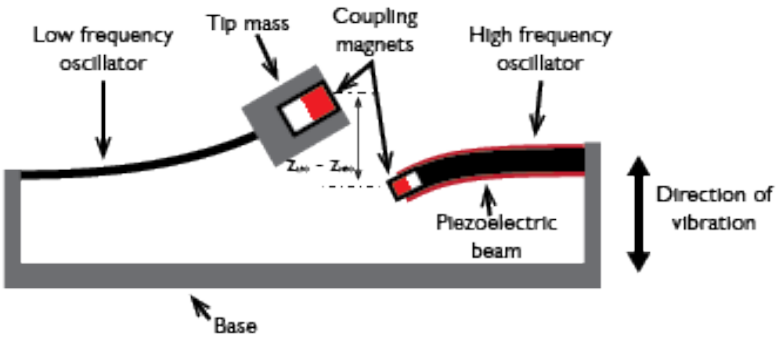

Figure 3.4: Initial schematic design consisting of two cantilever beams, of which one is a piezoelectric beam. These are coupled using magnets which pass eachother when set in motion.

described in table 3.1, with a render of the design found in figure 3.5.

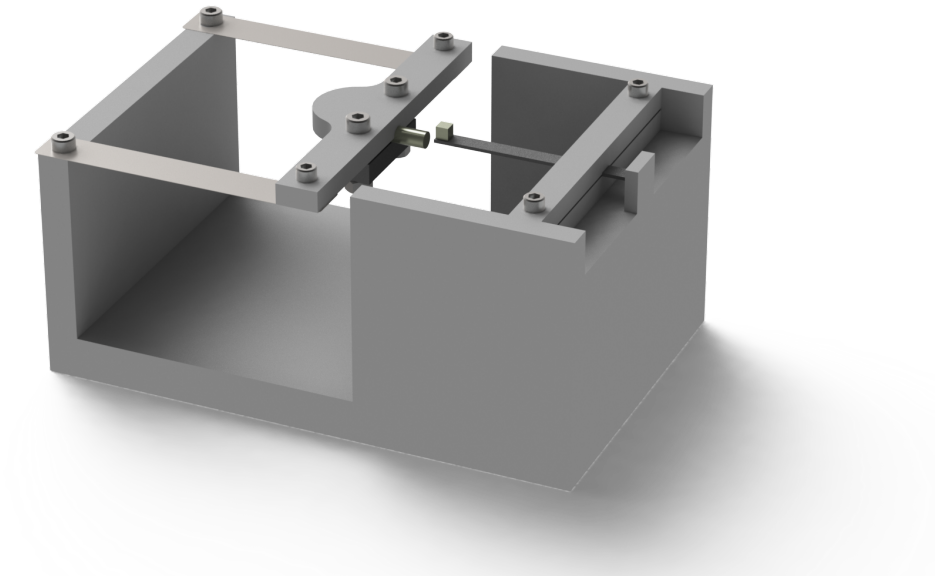

Figure 3.5: Render of the designed prototype.

3.6. MODELLING APPROACH

In this section a model for a frequency up-converted energy harvester will be presented. This model will give insight into the behaviour of such a system. The model will be based

Table 3.1: Prototype parameters

Parameter	Symbol	Value
LFO beam length	L_{LFO}	60 mm
LFO beam width	b_{LFO}	20 mm
LFO beam thickness	h_{LFO}	0.1 mm
LFO tip mass	M_{LFO}	14.24 g
HFO tip mass	M_{HFO}	0.19 g
HFO beam width	b_{HFO}	6 mm
HFO beam length	b_{HFO}	32mm
Distance between magnets	d_{gap}	2 mm
LFO beam density	ρ_{LFO}	7.9 g/cm^3
Substrate density	ρ_s	8200 g/cm^3
Piezo density	ρ_p	7800 g/cm^3
Substrate thickness	h_s	0.37 mm
Piezo thickness	h_p	0.19 mm
Capacitance single layer	C	36.22 nF
Elasticity Piezo	Y_{33}^E	61 GPa
Elasticity Substrate	Y_s	200 GPa
Piezoelectric constant	e_{31}	-19.2
LFO magnet dimension	-	4mm x 20mm
HFO magnet dimension	-	3 x 3 x 3 mm

around distributed parameters models derived from literature. The model is extended with the magnetic coupling between both cantilevers. First the beam equations will be described, after which the coupling between these beams will be described. Lastly the electromechanical coupling enabled by the piezoelectric cantilever beam will be described.

A schematic overview of the system is shown in figure 3.6. The described values in this schematic are the beam lengths (L_{HFO} & L_{LFO}), tip masses (M_{HFO} & M_{LFO}), the gap size (d_{gap}), and the input base motion (W_b). The cantilevers have two magnets connected at its free length, in order to couple both beams and enable a frequency up-conversion.

In order to return a valuable result a distributed parameter model was chosen. This is necessary in order to describe the electromechanical coupling, as well as to enable the magnetic coupling. The beams are expected to be resonating near their natural frequency, which results in certain modes to be dominant. A modal analysis can therefore be used, this will give further insight into the dynamic deflection and can be used to compute the electromechanical coupling.

Distributed parameter models have been extensively discussed in literature, as can be found in works by Lu et al [4] and Pillatsch [5]. However, more comprehensive work can be found in the models described by Erturk and Inman [6]. These form the basis for the analysis found throughout this chapter. Models described by Pillatsch [5] have also included the coupling between two magnets in order to determine tip force interactions with the model.

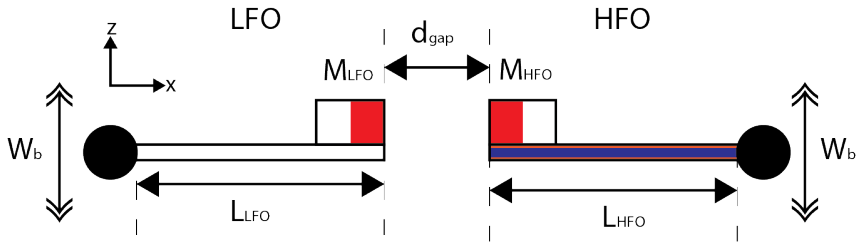

Figure 3.6: Schematic overview of the system to be modelled. Both fixed ends of the cantilevers are fixed to the same base. The high frequency oscillator consists of a piezoelectric beam with 3 layers.

3.7. CANTILEVER BEAM MODEL

The partial differential equation governing forced vibrations for a cantilever beam can be described as following, as was found in [6].

$$\begin{aligned} &-\frac{\partial^2 M(x,t)}{\partial x^2} + c_s I \frac{\partial^5 w(x,t)}{\partial x^4 \partial t} + c_a \frac{\partial w(x,t)}{\partial t} + m \frac{\partial^2 w(x,t)}{\partial t^2} \\ &= -\left[m_p + M_t \delta(x-L)\right] \frac{\partial^2 w_b(x,t)}{\partial t^2} + F(w) \end{aligned} \tag{3.1}$$

3.8. MODAL ANALYSIS

Where w is the transverse displacement of the beam relative to the base position. The parameters c_s and c_a are the strain rate damping and viscous air damping coefficients. The mass per unit length is described by m and the tip mass is described by M_t. The Dirac delta function is shown by $\delta(x)$, and $M(x,t)$ is the internal bending moment. Finally the term $F(w)$ is used to describe the force on the tip mass caused by the magnetic coupling. This internal bending moment can be used to remove the fourth order derivative term by using the following equation.

$$\frac{\partial^5 w(x,t)}{\partial x^4 \partial t} = \frac{\partial}{\partial t} \frac{\partial^2 M(x,t)}{\partial x^2} \tag{3.2}$$

In order to determine the internal moment both the piezoelectric and substrate layer have to be integrated for the axial stresses in the beam-cross section. The internal moment can thus be found by the following for the HFO, for the LFO the h_p value can be set to 0 as there is no piezoelectric layer.

$$M(x,t) = -b\left(\int_{-\frac{h_s}{2}-h_p}^{-\frac{h_s}{2}} T_1^p y \, \mathrm{d}y + \int_{-\frac{h_s}{2}}^{\frac{h_s}{2}} T_1^s y \, \mathrm{d}y + \int_{\frac{h_s}{2}}^{\frac{h_s}{2}+h_p} T_1^p y \, \mathrm{d}y\right) \tag{3.3}$$

Here b is the width of the beam, h_p and h_s are the layer heights of the piezoelectric layer and substrate layer, respectively. The T_1^p and T_1^s are the axial stresses in the piezoelectric layer and substrate layer, respectively. These can be computed using the Youngs modulus (Y), bending strain(S_1), piezoelectric constant(e_{31}), and electric field E_3 as following:

$$\begin{aligned} T_1^S &= Y_s S_1^S \\ T_1^P &= c_{11}^E S_1^P - e_{31} E_3 \\ S_1(x,y,t) &= -y\frac{\partial^2 w(x,t)}{\partial x^2} \end{aligned} \tag{3.4}$$

These equations can be substituted in equation 3.3, which will result in an moment described for a series connected piezoelectric cantilever beam as following:

$$M^s(x,t) = -YI\frac{\partial^2 w_{rel}^s(x,t)}{\partial x^2} + \theta_s v_s(t)[H(x) - H(x-L)] \tag{3.5}$$

Where YI is the bending stiffness, which will later be described. Here the coefficient of coupling (θ_s) can be determined by the evaluation of the following equation:

$$\theta_s = \frac{e_{31} b}{2h_p}\left[\left(h_p + \frac{h_s}{2}\right)^2 - \frac{h_s^2}{4}\right] \tag{3.6}$$

Furthermore the bending stiffness (YI) for a short-circuit condition of the piezoelectric cantilever beam can be described as following:

$$YI = \frac{2b}{3}\left\{Y_{\bar{s}}\frac{h_s^3}{8} + \bar{c}_{11}^E\left[\left(h_p + \frac{h_s}{2}\right)^3 - \frac{h_s^3}{8}\right]\right\} \tag{3.7}$$

Combining these results with equation 3.1 returns a resulting coupled beam equation as following for a series connected piezoelectric cantilever beam, which is easily reduced for a non piezoelectric cantilever beam like the LFO.

$$\begin{aligned} &YI\frac{\partial^4 w_{rel}^s(x,t)}{\partial x^4} + c_s I\frac{\partial^5 w_{rel}^s(x,t)}{\partial x^4 \partial t} + c_a\frac{\partial w_{rel}^s(x,t)}{\partial t} + m\frac{\partial^2 w_{rel}^s(x,t)}{\partial t^2} \\ &-\theta_s v_s(t)\left[\frac{d\delta(x)}{dx} - \frac{d\delta(x-L)}{dx}\right] = -[m - M_t\delta(x-L)]\frac{\partial^2 w_b(x,t)}{\partial t^2} \end{aligned} \tag{3.8}$$

Here the $v_s(t)$ term is the voltage response. The right hand side of the equation represents the base motion input to the system, later a tip force will be introduced in order to couple both oscillators. The mass per unit length (m) is described by the following equation:

$$m_\mathrm{p} = b\left(\rho_\mathrm{s} h_\mathrm{s} + 2\rho_\mathrm{p} h_\mathrm{p}\right) \tag{3.9}$$

Where ρ_p and ρ_s are the densities of the piezoelectric and substrate layer respectively.

When assuming a proportional damping the vibration response can be represented as a series of the eigenfunctions described by:

$$w(x,t) = \sum_{i=1}^{\infty} \phi_i(x)\eta_i(t) \tag{3.10}$$

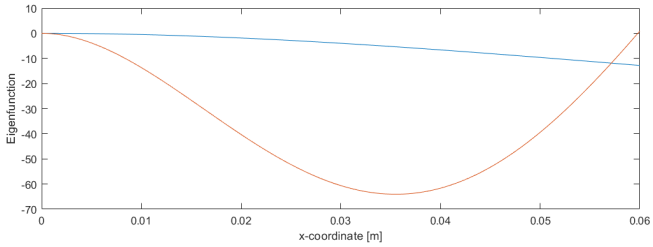

Figure 3.7: Mass normalised eigenfunction shapes of the first two modes for the low frequency oscillator.

Where $\phi_i(x)$ is the mass-normalised eigenfunction of the ith vibration mode, and η_i is the modal mechanical coordinate of the ith coordinate. The mass-normalised eigenfunctions can be described using the following equation, for the first two eigenmodes of the described system the eigenfunctions are plotted in figure 3.7 for the LFO.

$$\phi_i(x) = A_i\left(\cos\frac{\lambda_i}{L}x - \cosh\frac{\lambda_i}{L}x + \zeta_i\left(\sin\frac{\lambda_i}{L}x - \sinh\frac{\lambda_i}{L}x\right)\right) \tag{3.11}$$

Where λ_i is the modal eigenvalue of the ith mode, L the free beam length, and x the coordinate in the beam. With the parameter ζ_i defined as following:

$$\zeta_i = \frac{\sin\lambda_i - \sinh\lambda_i + \lambda_i\frac{M_t}{mL}(\cos\lambda_i - \cosh\lambda_i)}{\cos\lambda_i + \cosh\lambda_i - \lambda_i\frac{M_t}{mL}(\sin\lambda_i - \sinh\lambda_i)} \tag{3.12}$$

Where M_t, m_p, I_t are the tip mass and the beam mass per unit length respectively.

The modal amplitude constant (A_i) is found by finding a solution to normalising the eigenfunctions according to the following orthogonality conditions:

$$\int_0^L \phi_j(x)m\phi_i(x)dx + \phi_j(L)M_t\phi_i(L) + \left[\frac{d\phi_j(x)}{dx}I_t\frac{d\phi_i(x)}{dx}\right]_{x=L} = \delta_{ij} \tag{3.13}$$

$$\int_0^L \phi_j(x)YI\frac{d^4\phi_i(x)}{dx^4}dx - \left[\phi_j(x)YI\frac{d^3\phi_i(x)}{dx^3}\right]_{x=L} + \left[\frac{d\phi_j(x)}{dx}YI\frac{d^2\dot{\phi}_i(x)}{dx^2}\right]_{x=L} = \omega_i^2\delta_{ij} \tag{3.14}$$

However, solving for only the first should satisfy the second condtion and as such only the first will be solved. Here I_t is the mass moment of inertia of the tip mass M_t about the free end $(x = L)$. The Kronecker delta function is here described by $delta_{rs}$.

The undamped natural frequency of the ith vibration mode in short-circuit condition is described by:

$$\omega_r = \lambda_r^2\sqrt{\frac{YI}{m_\mathrm{p}L^4}} \tag{3.15}$$

The modal eigenvalue λ_i of the ith mode is found by solving the following general equation:

$$1+\cos\lambda_i\cosh\lambda_i+\lambda_i\frac{M_\mathrm{t}}{m_\mathrm{p}L}(\cos\lambda_i\sinh\lambda_i-\sin\lambda_i\cosh\lambda_i)$$
$$-\frac{\lambda_i^3 I_\mathrm{t}}{m_\mathrm{p}L^4}(\cosh\lambda_i\sin\lambda+\sinh\lambda_i\cos\lambda_i) \tag{3.16}$$
$$+\frac{\lambda_i M_\mathrm{t} I_\mathrm{t}}{m_\mathrm{p}^2 L^4}(1-\cos\lambda_i\cosh\lambda_i)=0$$

Something which should be mentioned in order to implement the model properly is the previously described model is given for short-circuit conditions, as such the load resistance connected to the piezoelectric beam is set 0Ω. This will cause the voltage output to vanish as this will go to 0.

Thus what can be concluded is the voltage response also returns a feedback to the mechanical response and as such will alter the resonance frequency.

A final part that has to be transformed in a similar manner is the input force, which has been described by the first part of the right hand side in equation 3.1. Transforming this using the same orthogonality conditions this results in the following equation, where a_c is the constant acceleration amplitude.

$$f_i(t)=-\left(m_p\int_0^L\phi_i(x)dx+M_t\phi_i(L)\right)a_c\sin\omega_b t \tag{3.17}$$

3.9. COUPLING FORCE

The coupling force in the model is described by a force acting on each mode. This is described by the following equation:

$$F_i(t)=\int_0^L\phi_i(x)f(x,t)dx \tag{3.18}$$

Which simplifies to the following when considering only a tip force:

$$F_i(t)=\phi_i(L)f(L,t) \tag{3.19}$$

However, in order to determine these forces ($f(L,t)$) the interaction of both magnets should be modelled. This was first performed using COMSOL. A detailed description of this process can be found in appendix A. This resulted in the following force-distance plot for different values of the gap size d_{gap}, which can be noticed in figure 3.8.

Different approaches were used to determine a proper fit to later use in the simulation of the complete model, as performing a FEM analysis for every time step is computationally expensive. Two approaches for approximating the force function were used, first a Gaussian approximation [5] and second a dipole force model [7].

The gaussian approximation is described by:

$$g_{fit}(z_{HFO}-z_{LFO})=-\frac{A}{C^2}(z_{HFO}-z_{LFO})\,e^{-\frac{(z_{HFO}-z_{LFO})^2}{2C^2}} \tag{3.20}$$

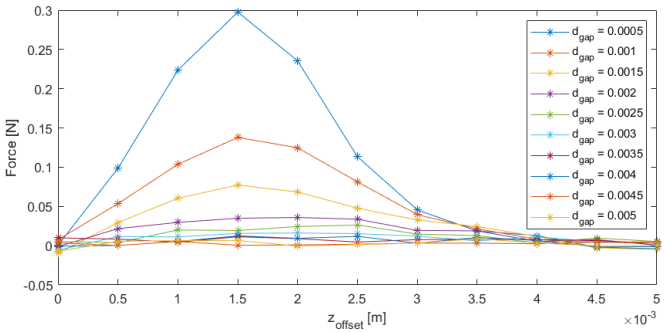

Figure 3.8: Force against perpendicular offset between magnets for different parallel distance sizes (gap distances). Results from COMSOL plotted using MATLAB.

Where A and C are the fitting parameters. The term $(z_{HFO} - z_{LFO})$ describes the distance between the tips of both cantilevers. For a gap size of 2mm the fitting parameters were determined to be as following.

$$A = -1.0607 * 10^{-4}$$

$$C = 1.7 * 10^{-3}$$

The dipole model has been described as following:

$$F_z = \frac{3\mu_0 \left(m_1 m_2 z_{off} - \frac{5 d_{dipole}^2 m_1 m_2 z_{off}}{d_{dipole}^2 + z_{off}^2} \right)}{4\pi (d_{dipole}^2 + z_{off}^2)^{\frac{5}{2}}} \tag{3.21}$$

Wherem_1 and m_2 were fitted using the in COMSOL obtained data. The value d_{dipole} is the distance between both dipoles, for the case where d_{gap} was set to 2mm this resulted in fit parameters to be as following:

$$m_1 = -8.4 * 10^{-4}$$

$$m_2 = 4.05 * 10^{-2}$$

Overall the dipole moment takes a longer time to compute, while the Gaussian function has a better approximation. This is the main reason for choosing the Gaussian approximation to work further with. Both approximations, as well as the simulation results are displayed in figure 3.9.

3.10. MECHANICAL DAMPING

The mechanical damping of the cantilevers is a value which is hard to determine analytically, while an experiment to determine one is easily performed. This is done by uncoupling the frequency up-conversion, and measure the impulse response of the tip displacement. By evaluating the decrement the damping ratio is easily obtained, this

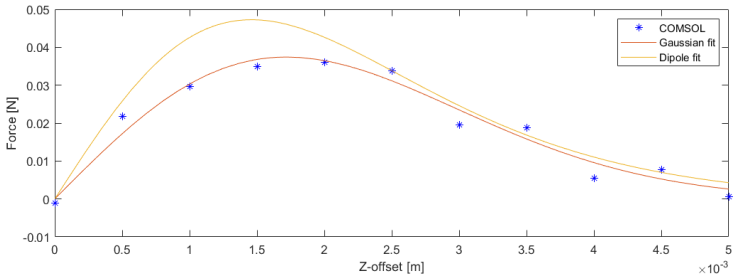

Figure 3.9: Force against perpendicular offset between magnets calculated using a FEM COMSOL model, the presented Gaussian approximation as well as the dipole model method for a gap size of 2mm.

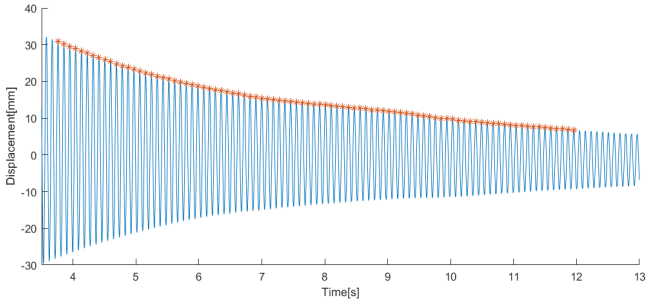

Figure 3.10: Ring down test results measured on the low frequency oscillator using a laser doppler vibrometer. Resulting in a damping ratio of 0.0028. The resulting time series for the displacement as well as its peaks are shown.

experiment was performed for both cantilevers. The results for these so called ringdown tests can be found in figures 3.10 and 3.11 for the LFO and HFO respectively. By determining the peak positions for every oscillation this can be fitted through the logarithmic decrement described as following:

$$\zeta = \frac{1}{2\pi} \ln\left(\frac{z_i}{z_{i+1}}\right) \tag{3.22}$$

The resulting damping conditions were found to be 0.0028 for the LFO and 0.0394 for the piezoelectric HFO in short-circuit conditions, while a damping ratio of 0.0361 was found in the HFO for open-circuit conditions.

3.11. EQUATIONS OF MOTION

Finally the previously found results can be combined into the governing equations of motion for the modal coordinates as following respectively for the LFO and HFO, where i and j stand for the ith and jth mode of the LFO and HFO respectively. Here F_i is given by equation 3.19, and f_i is given by equation 3.17.

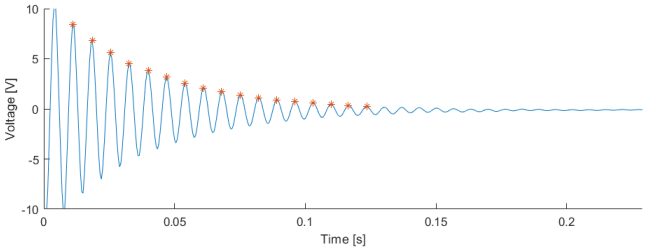

Figure 3.11: HFO ring down test results shown for the voltage response measured over a resistance of 4MΩ with a resulting computed damping ratio of 0.0361. The resulting time series for the voltage as well as its peaks are shown.

$$\frac{d^2\eta_i(t)}{dt^2} + 2\zeta_i\omega_i\frac{d\eta_i(t)}{dt} + \omega_i^2\eta_i = f_i(t) + F_i(t) \tag{3.23}$$

$$\frac{d^2\eta_j(t)}{dt^2} + 2\zeta_j\omega_j\frac{d\eta_j(t)}{dt} + \omega_j^2\eta_j - \theta_j v_s(j) = f_j(t) - F_j(t) \tag{3.24}$$

The electrical response can be described using the following equation:

$$C_p\frac{dv_s(t)}{dt} + \frac{v_s(t)}{R_l} + \sum_{j=1}^{\infty}\theta_j\frac{d\eta_j(t)}{dt} = 0 \tag{3.25}$$

3.12. IMPLEMENTATION

In order to simulate the behaviour of the system a the model was implemented in MATLAB. For this approach first a single beam, being plucked by a moving magnet was implemented. This approach has similarites to the system described by Pillatsch [5]. The parameters used were also from the works by Pillatsch, in order to verify the results. These results can be found in figure 3.12. These results show initial results close to what has been found by Pillatsch. A next step is to implement the parameter values from the design that has been made, using the newly found force approximation values and the parameters for the HFO to be used in the prototype. The results from this can be seen in figure 3.13. A significant difference is the orientation of the magnets, where the previously shown results have magnets in an attracting setup, whereas the current design uses a repelling setup. As these results show expected results for plucking behaviour the next step would be to excite the a single oscillator, which would represent the low frequency oscillator. These results are shown in figure 3.14. However, a next step would be to couple both systems. This step would prove to result in difficulties, which can be seen from figure 3.15.

The errors that have creeped into the implementation of the model were not solved during this thesis project, this will later be discussed in chapter 5. It can be observed that the plucking behaviour does happen, however the resulting motion is not as expected. This does also not correlate to the experimental results which will be described next.

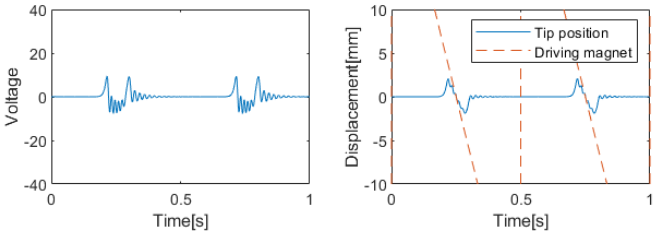

]

Figure 3.12: Simulated results for the high frequency oscillator plucked by a moving magnets, based on the works by Pillatsch [5]. Parameters used as found in [5].

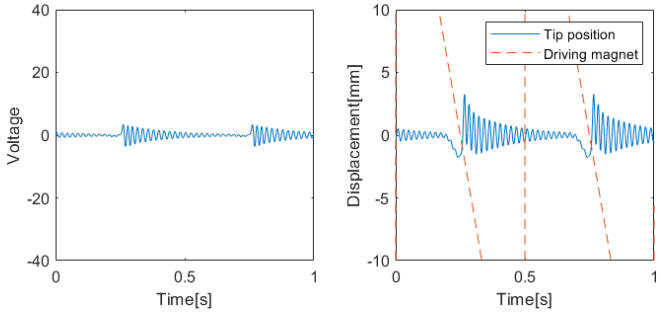

Figure 3.13: Simulated results for the high frequency oscillator plucked by a moving magnet under repelling condition, based on the parameters in the design.

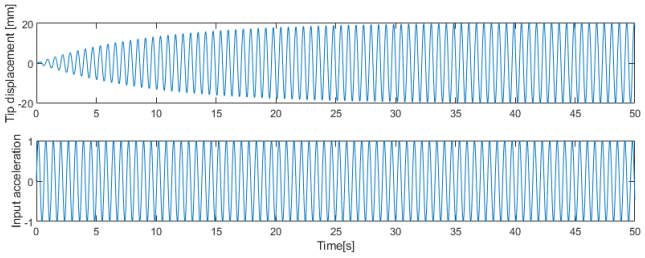

Figure 3.14: Simulated tip displacement for the uncoupled low frequency oscillator under a 10Hz 1g acceleration.

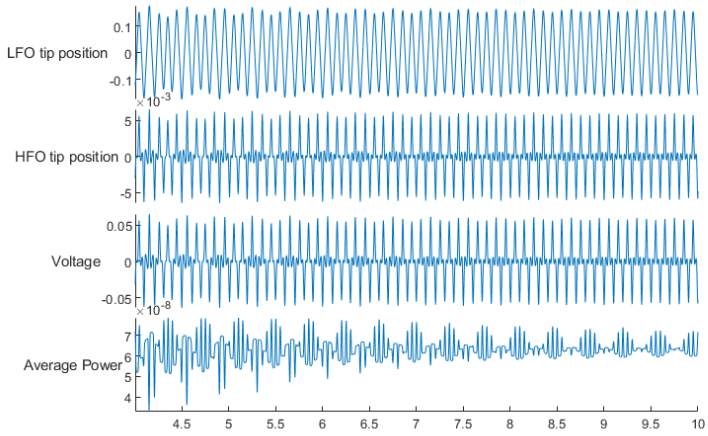

Figure 3.15: Time series result of the model under a 10Hz 1g acceleration input. Voltage output shown measured over a 1kOhm resistance.

REFERENCES

[1] T. Galchev, H. Kim, and K. Najafi, *Micro Power Generator for Harvesting Low-Frequency and Nonperiodic Vibrations,* Journal of Microelectromechanical Systems , 5961600 (2011).

[2] B. Andò, S. Baglio, V. Marletta, A. Pistorio, and A. R. Bulsara, *A low-threshold bistable device for energy scavenging from wideband mechanical vibrations,* IEEE Transactions on Instrumentation and Measurement **68**, 280 (2019).

[3] T. Galchev, E. E. Aktakka, and K. Najafi, *A Piezoelectric Parametric Frequency Increased Generator for Harvesting Low-Frequency Vibrations,* Journal of Microelectromechanical Systems **21**, 1311 (2012).

[4] F. Lu, H. Lee, and S. Lim, *Modeling and analysis of micro piezoelectric power generators for micro-electromechanical-systems applications,* Smart materials and structures **13**, 57 (2003).

[5] P. Pillatsch, E. Yeatman, and A. Holmes, *Magnetic plucking of piezoelectric beams for frequency up-converting energy harvesters,* Smart Materials and Structures **23**, 025009 (2014).

[6] A. Erturk and D. J. Inman, *Piezoelectric energy harvesting* (John Wiley & Sons, 2011).

[7] K. W. Yung, P. B. Landecker, and D. D. Villani, *An analytic solution for the force between two magnetic dipoles,* Magnetic and electrical Separation **9** (1998).

4

EXPERIMENTAL WORK

During the thesis project a prototype has been developed with the goal to verify the model. This prototype frequency up-converted energy harvester was subjected to a motion input on an electrodynamic shaker. This chapter will describe the built prototype, initial tests to prove the working of the system, and a frequency sweep test in order to gain data which can be used to compare against existing systems. Lastly the found data will be analysed, from which conclusions are drawn.

4.1. PROTOTYPE

The design of the prototype has been described previously in chapter 3. A small experiment was also included in this previous chapter, in order to determine the damping and gain insight in the natural frequencies of both oscillators. The prototype was then made, of which the process will be described here. Several design iterations have been made, including a small scale prototype, about which more can be found in appendix B.

The system and the naming convention of the different parts can be seen in figure 4.1. As can be seen the system will consist of two cantilever beams in parallel configuration for the low frequency oscillator, with a mass housing the magnet as a proof mass. The high frequency oscillator consists of a piezoelectric beam with a magnet attached using glue as its proof mass. The system shown has its magnets in a repelling configuration.

The base of the prototype is made of 3d printed PLA, connected with a bolt to the vibration exciter. On top of this bolt the accelerometer is attached. As it is not attached to the vibration exciter in figure 4.1, both this bolt and the accelerometer are not shown. On this base both the LFO and HFO cantilevers are attached on opposite sides. The piezoelectric beam of the HFO has a back plate in order to keep it consistently located. The LFO consist of two cantilevers, in order to have have a consistent alignment during motion. These LFO cantilevers have a shared tip mass connected in order to house the N38 neodymium cylindrical magnet with a diameter of 4mm and a length of 20mm. The HFO consists of a Morgan Ceramics PZT-508 of 46x6x0.8 mm, which has an N42 neodymium

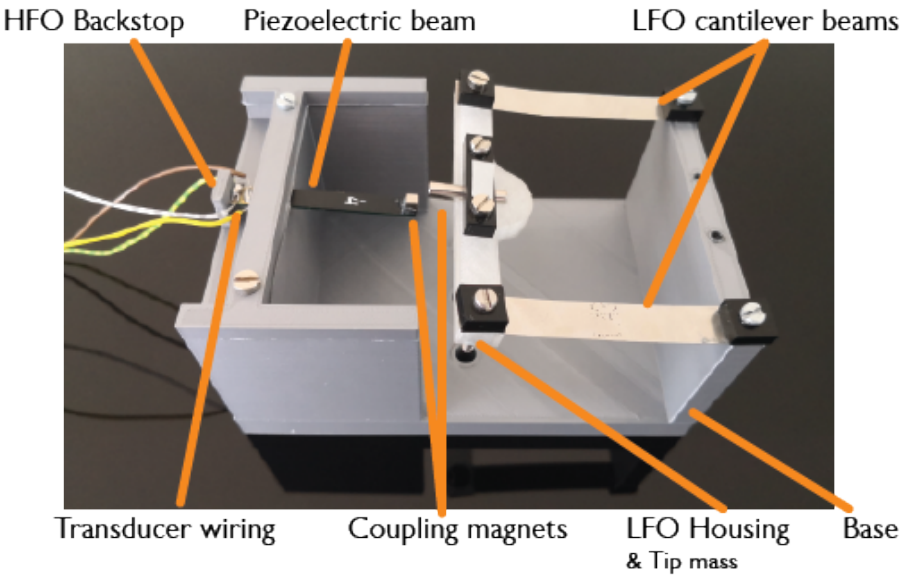

Figure 4.1: Picture taken of the final prototype which has been tested in this work. The main parts are labelled, with on the left hand side the low frequency oscillator and on the right hand side the high frequency oscillator.

cuboidal magnet with 3mm side lengths attached. The piezoelectric beam is series connected between the upper and lower layer. Further properties of the device are shown in table 4.1.

This prototype is used for all measurements in a repelling magnet configuration. From the ring down measurements performed in chapter 3 the first natural frequency in an uncoupled state can be computed. For the low frequency oscillator this was calculated to be 10.8 Hz, whereas the HFO piezoelectric beam in series connected to a resistance of 30 kΩ had a calculated frequency of 142.2 Hz.

4.2. ELECTRODYNAMIC SHAKER EXPERIMENTS

In order to perform measurements on different motion inputs an electrodynamic shaker was used. This shaker induces motion based on a voltage input. As the motion by the prototype results in feedback motion, a feedback controller was used based on the root mean squared values measured by an accelerometer.

In figure 4.2 the setup for the experiments is shown. An NI cRIO-9040 CompactRIO controller connected to a laptop running LabVIEW sends a voltage signal to the electrodynamic vibration test system, the TIRA TV51110, consisting of the shaker and an amplifier. The PCB 356A32 accelerometer returned its output in the direction of motion to an NI-9215 module on the controller in order to store the data and control the electrodynamic shaker making use of a feedback loop. Another voltage input to this module is the output from the laser doppler vibrometer sensor head, Polytec OFV-505, which is

Table 4.1: Prototype parameters

Parameter	Symbol	Value
LFO beam length	L_{LFO}	60 mm
LFO beam width	b_{LFO}	20 mm
LFO beam thickness	h_{LFO}	0.1 mm
LFO tip mass	M_{LFO}	14.24 g
HFO tip mass	M_{HFO}	0.19 g
HFO beam width	b_{HFO}	6 mm
HFO beam length	b_{HFO}	32mm
Distance between magnets	d_{gap}	2 mm
LFO beam density	ρ_{LFO}	7.9 g/cm^3
Substrate thickness	h_s 0.37 mm	
Piezo thickness	h_p	0.19 mm
Capacitance single layer	C	36.22 nF
Elasticity Piezo	Y_{33}^E	61 GPa
Elasticity Substrate	Y_s	200 GPa
Piezoelectric constant	e_{31}	-19.2
LFO magnet dimension	-	4mm x 20mm
HFO magnet dimension	-	3 x 3 x 3 mm

pre-processed by the vibrometer controller, Polytec OFV 2200. The voltage can be converted to displacement by multiplying with the displacement-voltage ratio of 5120 μm/V, as set on the vibrometer controller. Lastly, a voltage output from the prototype is measured. In order to do this the piezoelectric layers are in series connected, and the output is connected to a resistance substitution, Phipps & Bird Model 236A, on which a resistance can be set. Over this resistance the voltage is measured, which is the the last input to the compactRIO controller. The inputs to the compactRIO controller are stored on the laptop, in order to later be analysed.

4.3. CONSTANT FREQUENCY

A first measurement was performed to prove the working of the frequency up-converted energy harvester. This was done by having a harmonic input motion excite the prototype. The shaker motion was given a target motion of 10Hz under 1g acceleration. A partial result of this test can be seen in figure 4.3. During these tests it was found the laser vibrometer had a slight drifting over a longer period of time, for a short period of time this drift was acceptable for analysis.

From this figure it should be noted the acceleration measured on the base is not a perfect harmonic motion, as feedback from the high frequency oscillator causes a hard to control system. This should be taken into account for specific applications where this may not be desired. It can also be seen from the low frequency oscillator tip displacement that chaotic behaviour is happening. This happens as the low frequency oscillator is meant to overcome a threshold in order to pluck the system, however the low frequency oscillator sometimes does not have enough momentum to get over this thresh-

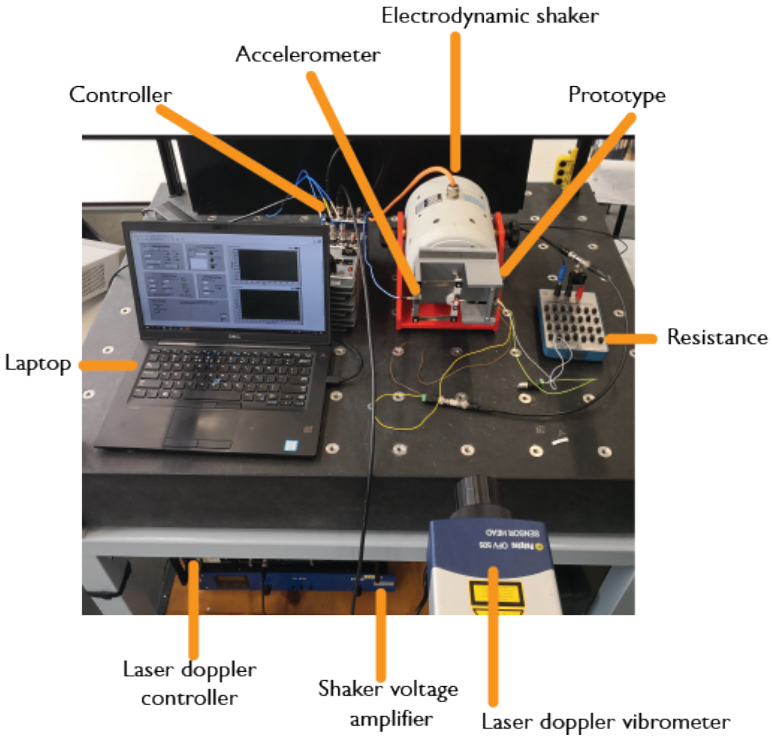

Figure 4.2: Complete setup of the experiment. The NI cRIO is connected to a computer in order to control the system. The electrodynamic shaker is controlled by the NI cRIO. The output measured by the NI cRIO are the laser doppler vibrometer, the voltage over the resistance box, and the acceleration signal. The acceleration signal is used for a feedback control loop in order to gain a constant acceleration amplitude.

old. This is seen by the difference between the height of the oscillation. The result is not having plucking behaviour at every input oscillation. However, from the voltage output it can be seen that irregularly plucking occurs. This is seen by the ringdown behaviour every so often. When looking at the low frequency oscillator tip positions it can be seen this plucking behaviour starts when the low frequency oscillator tip position moves past the middle position.

A further analysis can be made when looking at the fourier transform of the signals. The fourier transforms are shown in figure 4.4 for the acceleration, the low frequency oscillator tip position, and the voltage output.

From this a clear frequency up-conversion between the low frequency oscillator and the voltage output can be seen. The voltage output has a small peak at the same position as the input motion, as the high frequency oscillator is also excited with this motion. An even smaller peak at double this frequency is also seen, this is caused by the plucking behaviour as every period the plucking behaviour may occur twice. The large peak in the voltage output is at 138 to 146, which is in the vicinity of the natural frequency of the high frequency oscillator. The low frequency oscillator tip position has one dominant peak at 10 Hz, which is the similar to the input motion. However, the nonlinear

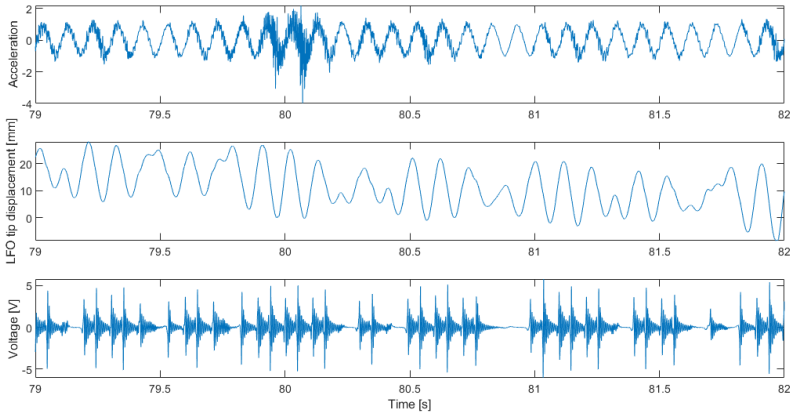

Figure 4.3: Partial time series result of the prototype under a 10Hz 1g acceleration input. The data measured is the base acceleration, the low frequency oscillator tip displacement, and the voltage output from the high frequency oscillator piezoelectric beam. Voltage output is measured over a 4 kΩ resistance.

chaotic behaviour of the system causes a lot of noise as well as secondary peaks. Similar secondary peaks are also observed in the voltage output. The acceleration signal has one frequency which is dominant, the target motion frequency of 10Hz. An up conversion ratio of approximately 14 is observed when analysing the peaks in both the voltage output and the LFO tip position.

4.4. FREQUENCY SWEEP

In order to give a better comparison over a broad range of frequencies, and to compare the performance of this prototype to other frequency up-converted energy harvesters a frequency up sweep was performed. Before testing a target range between 5Hz and 40Hz was set, however during testing it was observed the low frequencies resulted in poor feedback control performance. As such the frequency up-sweep was performed between 10Hz and 35Hz for a constant acceleration amplitude of 1g.

All three measured signals are shown in figure 4.5, from this it can be seen over a certain range the plucking behaviour happens. However, other results are difficult to interpret from this figure. It can be observed that the LFO displacement has a drift in its measurement, which has been previously discussed. Two more narrow regions are shown in figure 4.6, here both a region where a plucking occurs as well as a region where this does not occur is shown. From these figures it can be seen that when the LFO is unable to have a large enough displacement to the other side of the HFO the plucking behaviour does not occur. This motion is named intrawell motion. While during other moments the plucking does occur when the threshold is met for the LFO to pass the HFO, which is when interwell motion occurs.

A frequently used method of presenting the performance of frequency up-converted energy harvesters, or energy harvesters in general, is to show the root-mean-squared

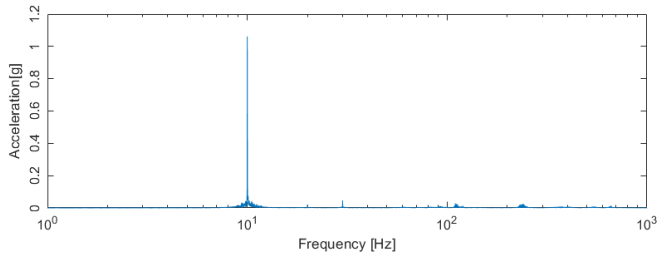

(a) Acceleration signal

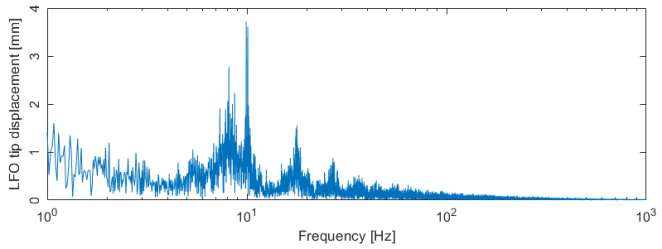

(b) Low frequency oscillator tip position

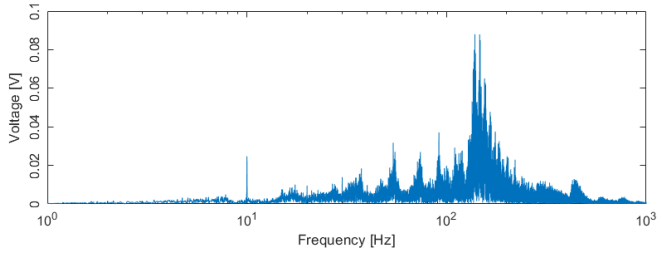

(c) Voltage output

Figure 4.4: Fourier transform for the measured signals for a target input of 1g 10Hz base motion.

power output and efficiency over the frequency range for which it has been measured. In order to show this the frequency is shown on the x-axis, which is converted from knowing this at the time shown in figure 4.5. This results in a figure where the x-axis contains the frequency, to show the performance of the system over the range of the frequency sweep. These are shown in figure 4.7, where the efficiency is shown as the generator figure of merit described in chapter 2.

From the power output it can be seen that over a certain frequency range between 11Hz and 14Hz, a significant power output is observed. This range is a so-called working range, however for slight changes in the measurement setup as well as the prototype different results for this graph will be obtained. The range is recurring, as well as the downward slope over this range. For the shown measurement a gap is seen, while this gap may shift when repeating the measurement. This is a direct result of cycles in which the plucking behaviour does not occur, which is chaotic. A direct explanation may be

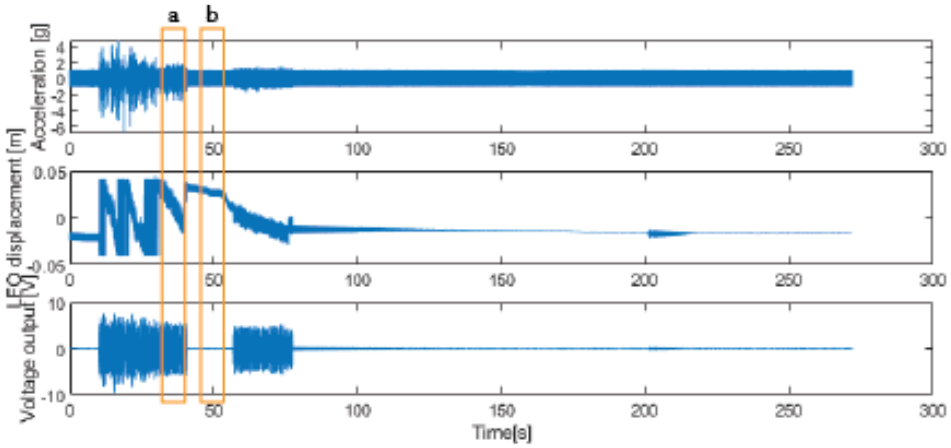

Figure 4.5: Measured signals for a frequency sweep between 10Hz and 35Hz at an acceleration amplitude of 1g. The outline regions are zoomed into in figure 4.6

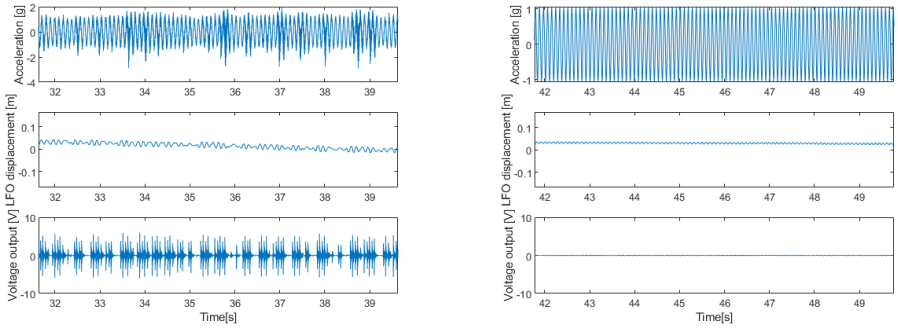

(a) Plucking behaviour region (Region a in figure 4.5)

(b) Non-plucking behaviour region. (Region b in figure 4.5)

Figure 4.6: Measured signals for a frequency sweep, zoomed in regions as shown in figure 4.5 in order to show more details. Both a region where the plucking behaviour occurs due to interwell motion as well as one where the LFO motion is limited to intrawell motion.

found when looking at the resonance frequencies for both interwell and intrawell motion. A peak generator figure of merit is found to be 0.106 at a frequency of 10.5Hz, with a normalised half efficiency bandwidth at 0.061. The moving root-mean-square of the voltage output is taken over a sampling time of 1.5s.

4.5. CONCLUSION

In this chapter it was shown the developed prototype shows frequency up-converted energy harvester behaviour, where a low frequency oscillator plucks the high frequency

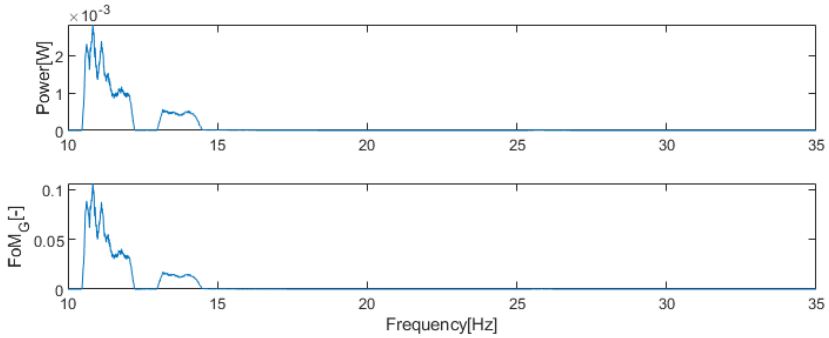

Figure 4.7: Calculated power and efficiency for a frequency sweep between 10Hz and 35Hz at an acceleration amplitude of 1g. The efficiency is shown in terms of generator figure of merit as described by Blad [1].

oscillating transducer. The behaviour is shown to be chaotic due to the nonlinear magnetic force. During interwell motion the plucking occurs, but a threshold has to be met. Otherwise intrawell motion occurs, which when resonated lets the low frequency oscillator have interwell motion again. For comparison a peak generator figure of merit is found of 0.106 at 10.5Hz, with a normalised half efficiency bandwidth of 0.061. In order to compare these values a comparison between this and other systems is given in table 4.2. From this table it is observed a decent peak efficiency is obtained, however the bandwidth is relatively low. Improvements to this system can be found by optimising the design parameters for a specific input motion. An improvement to the experimental work can also be made by using a measurement setup with a controlled frequency range that is more suiting to the design which has been fabricated.

Table 4.2: Comparison table between data found in literature to the values obtained during this thesis project.

Reference	FoM_g	BW_{nhe}
Dauksevicius [2]	0.037323	0.1589111
Dechant [3]	0.392887	0.4102603
Gu [4]	0.676432	0.1331748
Pillatsch [5]	0.65	3.08
Galchev [6]	0.19	2.34
Galchev [7]	0.27	0.549
Tang [8]	0.00391	0.374
Ashraf [9]	0.61	0.0704
This work	0.106	0.06

REFERENCES

[1] T. Blad and N. Tolou, *On the efficiency of energy harvesters: A classification of dynamics in miniaturized generators under low-frequency excitation,* Journal of Intelligent Material Systems and Structures **30**, 2436–2446 (2019).

[2] R. Dauksevicius, D. Briand, R. Lockhart, A. V. Quintero, N. de Rooij, R. Gaidys, and V. Ostasevicius, *Frequency up-converting Vibration Energy Harvester with Multiple Impacting Beams for Enhanced Wideband Operation at Low Frequencies,* Procedia Engineering **87**, 1517 (2014).

[3] E. Dechant, F. Fedulov, D. V. Chashin, L. Y. Fetisov, Y. K. Fetisov, and M. Shamonin, *Low-frequency, broadband vibration energy harvester using coupled oscillators and frequency up-conversion by mechanical stoppers,* Smart Materials and Structures **26**, 065021 (2017).

[4] L. Gu and C. Livermore, *Impact-driven, frequency up-converting coupled vibration energy harvesting device for low frequency operation,* Smart Materials and Structures **20**, 045004 (2011).

[5] P. Pillatsch, E. M. Yeatman, and A. S. Holmes, *A scalable piezoelectric impulse-excited generator for random low frequency excitation,* in *2012 IEEE 25th International Conference on Micro Electro Mechanical Systems (MEMS)* (IEEE, Paris, France, 2012) pp. 1205–1208.

[6] T. Galchev, E. E. Aktakka, and K. Najafi, *A Piezoelectric Parametric Frequency Increased Generator for Harvesting Low-Frequency Vibrations,* Journal of Microelectromechanical Systems **21**, 1311 (2012).

[7] T. Galchev, H. Kim, and K. Najafi, *Micro Power Generator for Harvesting Low-Frequency and Nonperiodic Vibrations,* Journal of Microelectromechanical Systems , 5961600 (2011).

[8] Q. C. Tang, Y. L. Yang, and X. Li, *Bi-stable frequency up-conversion piezoelectric energy harvester driven by non-contact magnetic repulsion,* Smart Materials and Structures **20**, 125011 (2011).

[9] K. Ashraf, M. Md Khir, J. Dennis, and Z. Baharudin, *Improved energy harvesting from low frequency vibrations by resonance amplification at multiple frequencies,* Sensors and Actuators A: Physical **195**, 123 (2013).

5

REFLECTION AND CONCLUSION

This chapter reflects on the research performed during the graduation project. This includes the literature review as well as the thesis research. A more in depth analysis of the activities is discussed, including the unsuccessful ones. A number of general conclusions are discussed as well as recommendations for future works.

5.1. RESEARCH ACTIVITIES

Over the course of the thesis project the research objective has changed. From initially looking into the effects of varying FupC specfic design parameters as presented in the literature study to presenting a novice device enabling frequency up-converted energy harvesting which has been experimentally tested.

During the thesis project first a general knowledge was obtained on the topic of vibration energy harvesting, leading to the insight of edge cases which seem most interesting. A specific field to look into was the field of frequency up-converted energy harvesters, as this was expected to result in research with most impact. This was due to the applications that were identified.

After this a literature review was conducted on the topic of frequency up-converted energy harvesters, during which FupC specific design variables were identified. These variables were useful for insight when comparing different systems, and as such a next goal was set. Namely identifying the effects of different FupC specific design variables on the performance of these systems.

The goal to determine the effects of FupC specific design parameters was a direct follow up of the literature review, which had interesting results and as such made the research goal an interesting one. However, while looking further into the effects it was observed these variables can not be analysed without altering other parts of the system. This did show the necessity of optimising a system as a whole for certain applications.

The focus shifted from the previously set goal to presenting the system that had been designed for which to test the sensitivities. This system has been fabricated, assembled, and afterwards experimentally tested. The resulting performance metrics have been presented.

The full thesis project work is visualised in figure 5.1

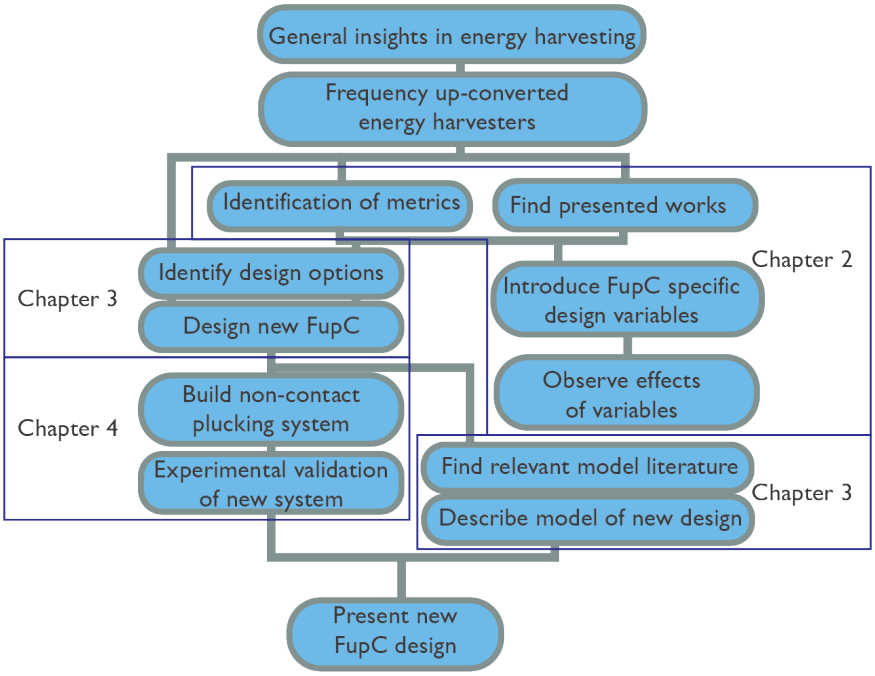

Figure 5.1: Overview of the research activities performed during the thesis project

5.2. DISCUSSION

The frequency up-converted specific design variables that have been identified during the literature study work as a method for comparison. During the thesis project the goal of gaining a more in depth understanding of the effects of these design variables was not fully met. This was caused by having seen that these parameters could not be changed without the requirement of changing other parameters in order to optimise the system. The method for frequency up-converted energy harvesting which has been developed can be used for further research and designs. It has been shown a frequency up-conversion happens, which has been shown to result in higher efficiencies for high motion ratios.

The developed model has not been correctly implemented, while steps have shown results as expected. The fault in the implementation may have been caused by a number of reasons. First an error in the differential equation solver was expected, which has been tested by changing the parameters. This did not seem to improve the results. Another issue may have been a parameter problem, as this may cause the high frequency oscillator to behave badly. Finally a wrongful MATLAB code may have been the cause, where a calculation is not performed as expected. While all parts have been tested individually, as well as showing that small steps result in expected behaviour, the error could

not be found. The model is not expected to be wrong, as parts have shown to describe parts of the system. These steps include both a coupling between a moving magnet and a plucked piezoelectric beam, as well as exciting a cantilever beam.

From the design process it was determined other configurations have yet to be designed. These included the works in this thesis project, as well as a configuration where there was a non-contact plucking event happening at the end of the LFO motion. Other distinctions have been determined during the process, and a more extensive morphological analysis may result in new designs while a lot of work has already been performed in this field. A new future design should also include experimental validation in order to proof the concept.

The thesis project did not have as a goal to design an optimised system, which could have been performed better when the developed model had a closely related implementation. The goal of gaining more insight into frequency up-converted energy harvesters and the effect of parameters has been met. As altering the magnetic coupling force, both in the MATLAB model with a moving magnet and in the prototype, resulted in different behaviour. Having a higher coupling force in a repelling configuration meant having a higher barrier to overcome in order to make plucking happen, however when this happened a higher initial amplitude of the HFO would be reached. This then resulted in a higher voltage output, which is as expected. A downside to this would be having a higher threshold for plucking, meaning the plucking behaviour will occur in a more narrow bandwidth and acceleration amplitude.

Lastly the comparison between previous work to the developed prototype was made. This showed a decent peak efficiency. For a system which has not been optimised, nor did this project have the goal to develop an optimised system, this is already a promising result. The high peak efficiency is a trade off between different parameters, and the most important one would be the bandwidth. The bandwidth computed from the experimental work during this thesis project was shown to be relatively low. However, a half efficiency bandwidth may not always be the goal and a different bandwidth definition, such as the working range, could be used to gain different insights. The half efficiency bandwidth will disadvantage systems with a relatively high peak efficiency, resulting in a conclusion to always be cautious of performance parameters.

5.3. RECOMMENDATIONS

My first recommendation would be to build a model based on presented and experimentally validated systems. From these a basis can be formed, and by adding in incremental steps your own research it should also be more clear where possible errors may occur. A second recommendation would be to document the experiments you perform as rigorous as possible, write all steps down in order to later faster redo the measurements. A third recommendation which worked well for me, look into what is available. Often a lot of materials are readily available in your environment, whether this is at home or in a lab environment. These make development faster. Lastly, I would recommend ask for the help of others around you. This could be during the manufacturing, design, or modelling, but also about choices with regards to your research objective. A fresh look into different parts will help more than your own mind might be able to at those moments.

5.4. CONCLUSION

The previously mentioned conclusions found in both the literature review as the final project are below summarised, as well as some additional conclusions that have appeared during the graduation project.

From the literature review it was found that presented work often has missing data in order to properly compare different systems to one another. The data presented in these works should contain frequency sweep results or probed frequency test results.

Generally a higher bandwidth has been observed in plucking based systems, while these also often have a steep drop-off outside a working range. Especially compared to impact based systems, which will have a longer transition phase generally.

The identified frequency up-converter specific design variables have been identified as the frequency ratio and mass ratio. While these result in interesting comparison methods for different systems, these should not be used to optimise a system to or identify performance improvements by adjusting these. More work should be analysed with complete data in order to observe patterns in detail.

During the graduation project it was found currently a lot of research has been and is being performed in the direction of frequency up-converted energy harvesters. However, these more often than not choose to incorporate nonlinear behaviour or difficult to compare coupling or oscillation methods. The work done in this project should provide a basis for future work to build on, as an improved implementation of the model should be achievable. As well as using different mode shapes or parameters in the model.

The frequency up-conversion method designed during this thesis project work was able to perform frequency up-conversion using a plucking based non-contact magnetic interaction between a low frequency oscillator and a high frequency oscillator acting as a transducer. This method can be further improved to be developed for research but also for industrial applications in various fields. The method is described by a model, which when implemented correctly can be used to optimise the system.

A

COMSOL MODEL OF THE MAGNETIC PLUCKING FORCE

In order to determine the forces between two magnets a FEM analysis was chosen, this analysis was performed using COMSOL. This approach models two static magnets over a number of positions in order to result in force-position data to use in the simulation of the proposed frequency up-converted energy harvester.

A.1. MODEL

In the COMSOL Multiphysics interface the 'Magnetic Fields, No Current' physics package was used. The two aligned magnets are a 3mm cuboid and an cylindrical magnet with a 4mm diameter and a 20mm length. As the model will remain aligned over a symmetric axis the model can be reduced to split at the half-way plane of the magnets. A bounding box around the magnets represents the material around the magnets through which the magnetic field flows. A geometry build can be seen in figure A.1. In order to perform the parameter sweep, the cuboid magnet will be displaced.

There have been three materials introduced, one for each of the magnets and one for the bounding box. The magnet materials both have a relative permeability set to 1.05, while the bounding box material has a relative permeability set to 1.

A.1.1. PHYSICS SETTINGS

The physics settings consist of three parts. First the boundary conditions were set, including the conditions required for the splitted geometry. These consist of a magnetic insulation on the sides of the boundary box excluding the side which was split, initial values with a magnetic scalar potential of 0A, and zero magnetic scalar potential on the side which was split.

Second, the magnetization of both magnets had to be set. These were set to 955 kA/m for both magnets, in order to get the results for repelling magnets this value has to be sign inverted for one of the magnets. This magnetization direction of both magnets is

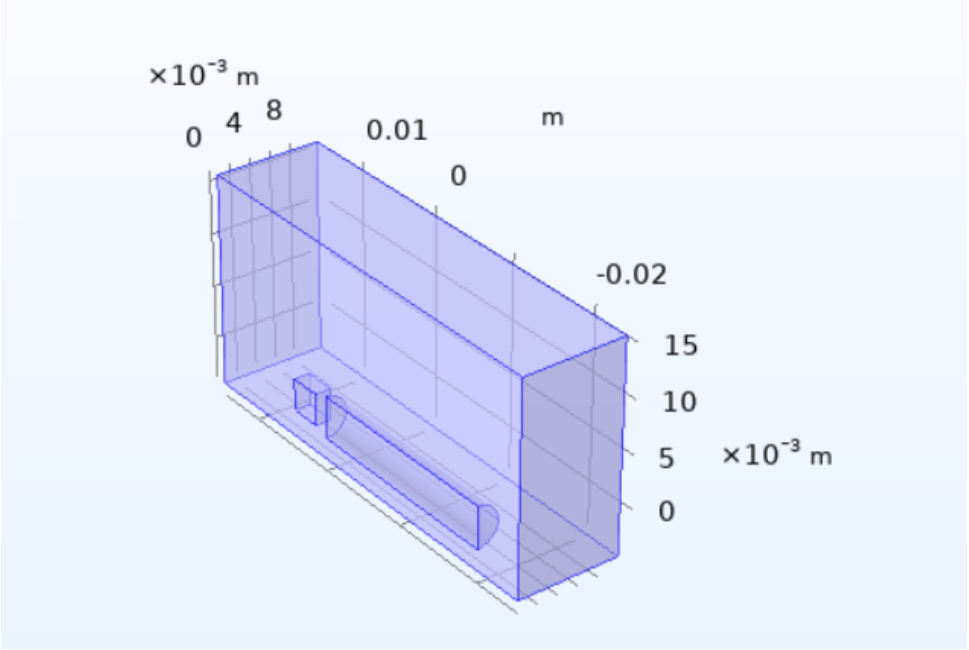

Figure A.1: Geometric setup in the COMSOL Multiphysics setup.

displayed in figure A.2.

Lastly, the force calculation had to be set up in order to gain results. This force calculation was measured on the cylindrical magnet, as this is a force acting between both magnets the force should be the same for both magnets.

A.2. STUDY

A double parametric sweep was taken, where the position of the cuboid magnet was updated during every step. The cuboid magnet moved in one direction parallel to the magnetization direction of both magnets, as well as a perpendicular direction in the plane of the geometric split. The parallel direction was set as a gap distance, ranging between 0.5mm to 5mm in 0.5mm intervals. While the perpendicular direction was measured over a range between 0mm and 5mm, with an 0.5mm interval.

A.3. RESULTS

In order to account for the split geometry the resulting forces have to be multiplied a magnitude of 2. Figure A.3 sums up the results found in the COMSOL study. These are for one direction of displacement. These values can later be used for the implementation of the frequency up-converted energy harvester.

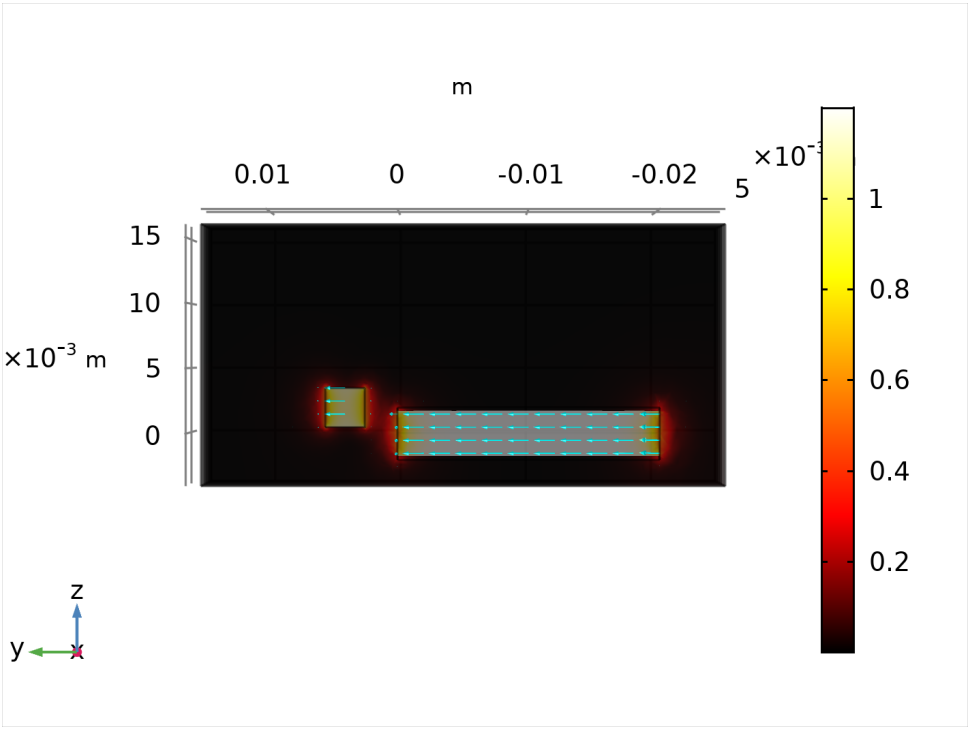

Figure A.2: Direction of magnetization of both magnets. Arrows show direction of magnetic flux density, colormap shows the magnetic flux density norm.

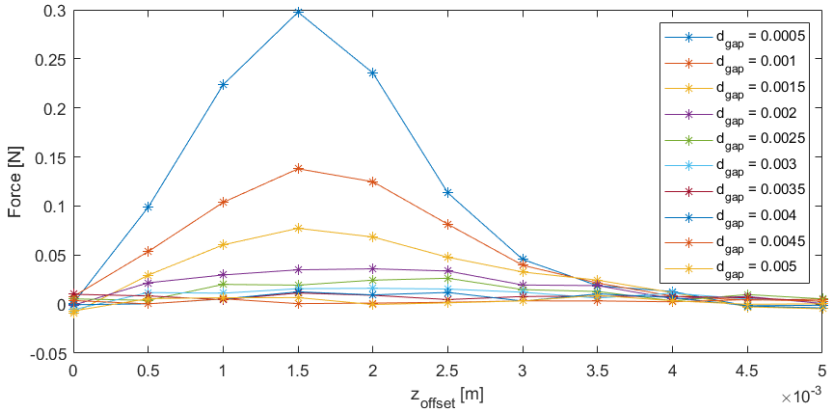

Figure A.3: Force against perpendicular offset between magnets for different parallel distance sizes (gap distances). Results from COMSOL plotted using MATLAB.

B

DESIGN ITERATIONS

As described in chapter 3 a design has been made, however a couple of iterations has been made to come to this design. This appendix will describe the fabrication method and show the design iterations. First the fabrication method will be described for the prototype described, then a few design iterations will be shown and their improvements will be discussed. Lastly a small scale model will be shown, which has also been tested. However due to design parameters not being optimised for this model the plucking behaviour wasnt as expected.

B.1. FABRICATION

In this section the fabrication of the different parts is described. First the naming convention is shown in figure B.1. Here the base is what all parts are attached to, and which is the only part connected to the electrodynamic shaker. The LFO beams are the cantilevers which oscillate with a LFO tip mass connected, this consists of two main parts namely the magnet and the housing. Second the HFO beam is shown, which is a piezoelectric beam with a tip mass consisting only of a magnet. The HFO beam is held in place by a fixture on top, and a resting plate at the back end.

The base is a 3D - printed PLA part with a 50% infill. This part was printed on a Prusa i3 mk3s. The same method of fabrication was used for the HFO fixture. For the LFO tip mass housing a similar approach was used, however for different design iterations different infills were used. This was done with the intent of having differing masses, however the net total was relatively low compared to the total mass. The experiments presented have used an infill of 25% for the LFO housing.

In order to connect the LFO beams to the base a set of PMMA with a thickness of 5mm was laser cutted. These function as load distribution with an edge at the same position as the edge of the base. The same connection method was used between the LFO beams and the housing. The magnet in the LFO housing was held in place using different methods, which will later be described in the design iterations. When a seperate fixture was used, as opposed to clamping, a PMMA block with a 5mm thickness was used again.

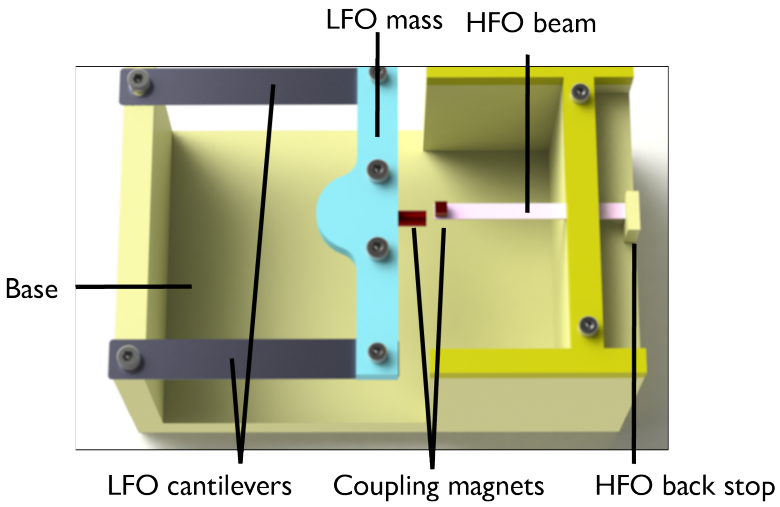

Figure B.1: Render of the prototype with the names used in this thesis report.

The piezoelectric beams are made by Morgan Ceramics from PZT-508. These are cut in a rectangular shape with at the end wires soldered on in order to connect to an output. The magnet is attached using glue.

B.2. SYSTEM ITERATIONS

A first system was a simple model of which a render can be seen in figure B.2. This system consists of two opposing cantilever beams, with a magnet which would be attached using glue on top of both tip ends. This system would be improved as the LFO is expected to have a tendency to twist. This brings us to the second iteration, which has two beams splitted at the LFO side. The result can be seen in figure B.3, as can be observed this already shows a close connection to the final system. However, when looking more into the fabrication method and the available resources an adjustment was made for the length of cantilever beams. This is seen in the final design in figure B.4.

B.3. BASE ITERATIONS

The base of the system has changed together with the complete model, however some base specific design iterations have been made and designed. First a base was made without keeping in mind the attachment position of the accelerometer, which was then placed underneath the LFO tip mass and in turn interfered with the performance of the system. This first model can be seen in figure B.5. An adjustment was to have holes to attach the accelerometer to on top of the base, on the same flat surface where the LFO beams are connected. This base was the system with which the experiments were conducted. This can be seen in figure B.4 A further improvement was designed but not fully tested, as the design had adjusted all parts, which proved to be time consuming to redo. This final improvement focused on decreasing the footprint of the base, while also

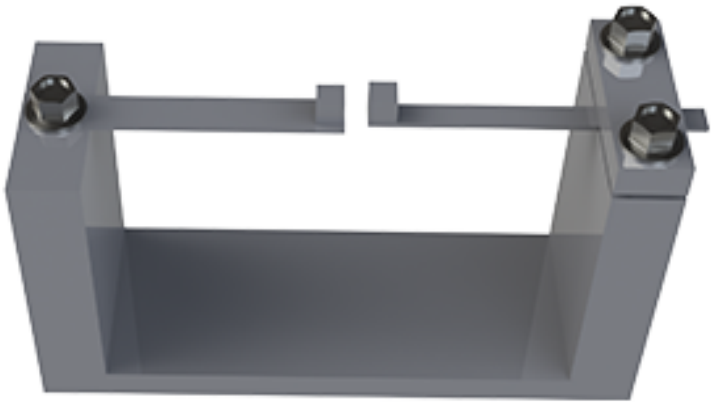

Figure B.2: Render of the initial design iteration.

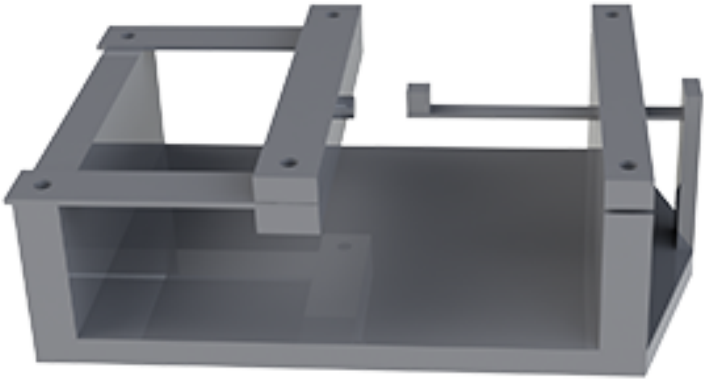

Figure B.3: Second design iteration of the prototype designed for this thesis project.

having a new position for the accelerometer in order to decrease the effect of the system dynamics on this sensor. The final resulting design can be observed in the render shown in figure B.6.

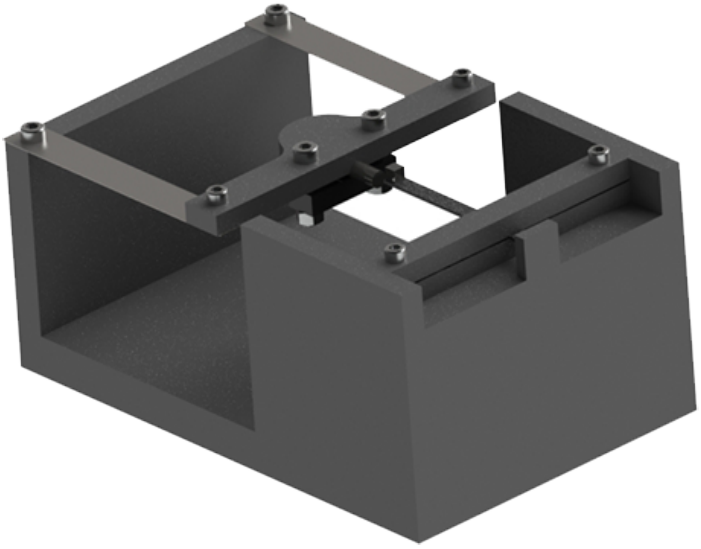

Figure B.4: Final design of the system designed during this thesis project. This model was produced and tested, the results of which have been presented.

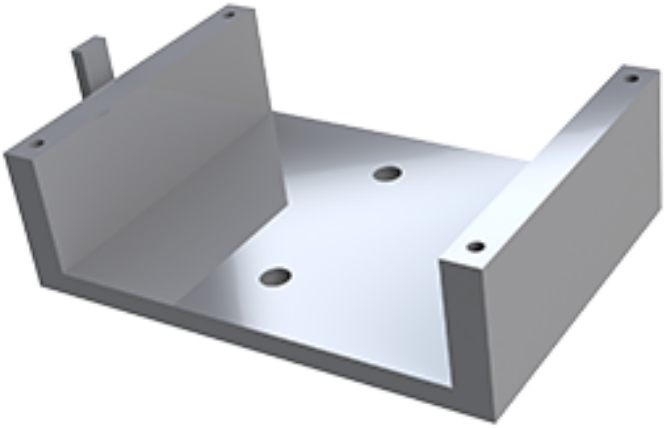

Figure B.5: Render of the initial base design, where the connecting holes were also used to attach the accelerometer sensor to. This proved to be too close to the LFO, and as such adjustments have to be made.

B.4. LFO ITERATIONS

As previously mentioned the first design consisted of a system which had all magnets glued to the respective beams. As this would have removed the ability to test both re-

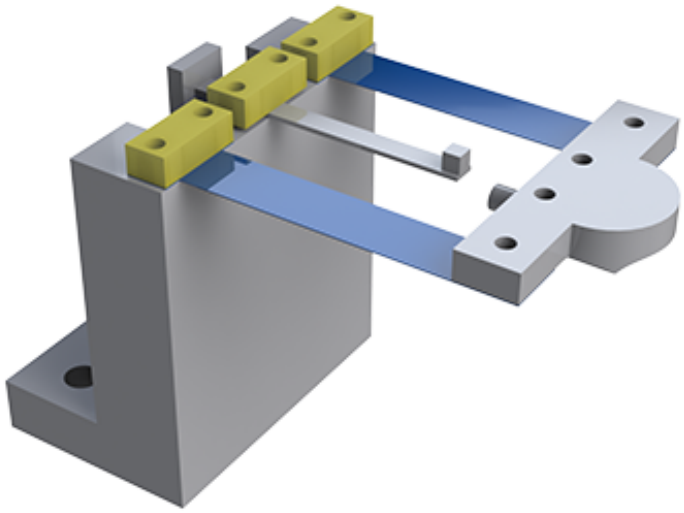

Figure B.6: Render of an improved design, where both oscillators share the same flat surface on the base. This would reduce footprint, however due to resource constraints was not fully developed.

pelling and attracting configurations, as well as noting the second design consisting of two cantilever beams requiring a connection between them a housing was designed. In the first design, which is seen in figure B.3 the magnet was aimed to be fitting well and would be kept in place in this manner. Another feature to notice is the method of connecting the LFO beams to the housing, as these were aimed to be clamped, with a fastener pushing inwards. The clamping would prove to leave a gap, while the magnet was easily pulled out of the housing in an attracting magnet configuration. A second design was later made to house both a larger magnet, and clamp the LFO beams in a similar manner as was done on the base. The resulting LFO housing part can be seen in figure B.7, where the magnet is clamped down in a slot.

B.5. SMALL SCALE DESIGN

In order to test in more significant motion ratios using the electrodynamic shaker a small scale design was proposed, designed, and built. The resulting small scale system can be seen in figure B.8. This small scale model had no piezoelectric beam, which also proved to be the main issue. At first it was thought a piezoelectric foil could be used to place on top of the HFO beam to transduce energy. However, research performed on this method proved this method would be time consuming and would not necessarily result in proper results as the piezoelectric film was too weak for this application. The method would be useful for a proof of concept if this is a goal of a research.

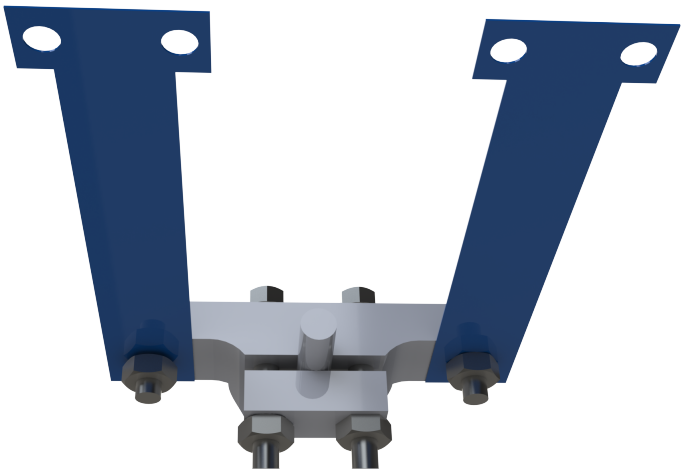

Figure B.7: Render of the LFO oscillator, including the housing, cantilever beams, and coupling magnet. This system clamps down the magnet in a keyhole in order to keep this in place.

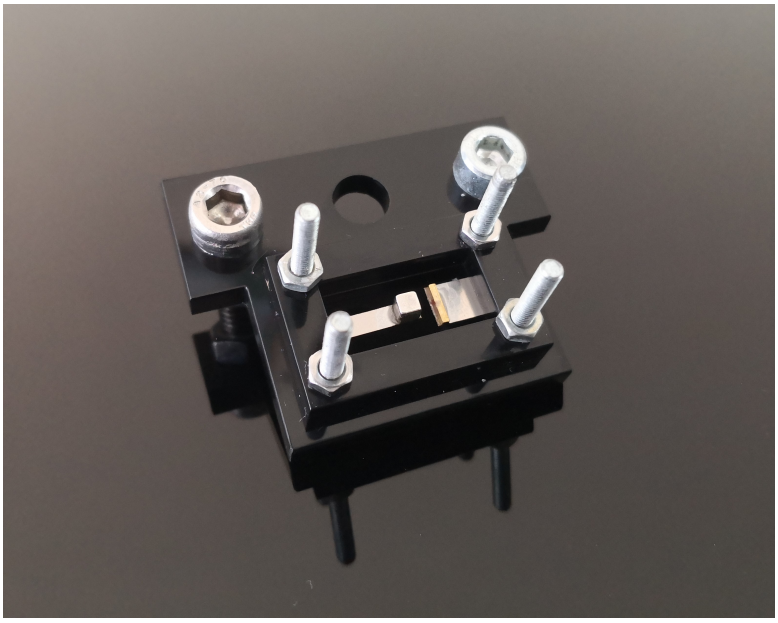

Figure B.8: Photograph of the small scale prototype, which was built during this thesis project. There is no transducer attached, nor is the coupling efficient. For these reasons the system was not tsted.